Journal of Constructional Steel Research 214 (2024) 108425

Contents lists available at ScienceDirect

Journal of Constructional Steel Research

journal homepage: www.elsevier.com/locate/jcsr

Post-fire assessment of composite steel-concrete box-girder bridges: Lessons from a recent incident

Juan José Pagán-Martínez [a], Ignacio Paya-Zaforteza [b,*], Antonio Hospitaler-Pérez [b]

[a] Universitat Politècnica de València, Spain
[b] ICITECH, Universitat Politècnica de València, Spain

ARTICLE INFO

Keywords:
Post-fire assessment
Post-fire repairs
Bridge fires
Composite box-girder
Forensic engineering

ABSTRACT

The structural fire analysis of bridges is crucial for ensuring transportation infrastructure safety since bridges, due to their unique characteristics and exposure to environmental hazards, are particularly susceptible to fire-induced damage. Despite this vulnerability, there is a lack of both experimental research and design guidelines for ensuring fire safety in bridges. This underscores the importance of studying actual bridge fire incidents.

This article presents a comprehensive examination of the numerical and experimental investigations carried out to evaluate the structural condition of a composite box-girder bridge located in Valencia, Spain, following a significant fire incident. In addition, the paper details the repair works carried out to fully restore the operational capacity of the bridge, along with the key lessons learnt from the incident. Therefore, the article highlights the vital synergy between advanced numerical models and experimental investigations to strengthen rehabilitation action plans and gain valuable insights for making informed decisions regarding post-fire structural integrity. By doing so, the study enhances understanding of bridge safety under fire and provides actionable recommendations for researchers, practitioners, and transportation authorities.

1. Introduction

Bridges play a critical role in transportation networks and their failure can have severe economic and human consequences, as evidenced by past incidents as proved, e.g., by the Morandi Bridge collapse in Genoa, Italy [1] or the I-35 W Mississippi bridge collapse in Minneapolis, USA [2]. While bridges are designed to withstand extreme events like earthquakes, there is a notable lack of guidance in current codes with respect to fire hazards [3,4]. This is concerning given the frequency of bridge fire events and their significant impact on infrastructure. For example, the MacArthur Maze collapse [5] in Oakland, California, on April 29, 2007, caused by a tanker truck fire, resulted in severe economic and social consequences. The transportation disruptions caused significant delays and increased costs for businesses and commuters, impacting regional commerce and trade. The economic impact of the collapse was estimated to be between $2 million and $4 million per day [6]. The explosion of a truck on the Kerch road bridge in Crimea on October 8, 2022 provoked the collapse of two bridge spans and set fire to several fuel tankers on the adjacent railway bridge, which also suffered an important damage [7]. The bridge was a vital logistical link for the Russian military [8] and the incident greatly impacted Russian's ability to transport troops and supplies to Crimea. More recently, on June 11, 2023, a vehicle fire under the I-95 highway near the Cottman Avenue exit in Northeast Philadelphia caused a portion of the highway to collapse, resulting in the closure of a segment that carried around 160,000 vehicles per day, of which roughly 14,000 were trucks [9]. Notable incidents such as the outlined above highlight the urgency of addressing fire safety in bridge design, and the need for proactive measures to prevent and mitigate such incidents in the future.

Compared to tunnel or building fires, which have been extensively studied in the literature (see e.g. [10–15]), bridges possess distinctive structural characteristics and require specialized analysis as highlighted in the comparison of key distinctive parameters of bridge, tunnel, and building fires conducted by Alos-Moya et al. [16]. This specialized analysis requirement combined with the importance of bridge fires and the lack of standards has spurred considerable research efforts over the past decade, as evident in the literature reviews conducted by Garlock et al. [3], Hu et al. [17], Liu et al. [4] and Nicoletta et al. [18]. A thorough analysis of these works reveals important gaps in the current body of knowledge. First, most of the existing studies rely on numerical models to theoretically analyze bridges fire response, but these models are not supported by a specific experimental validation. Second,

* Corresponding author.
E-mail addresses: juapagma@alumni.upv.es (J.J. Pagán-Martínez), igpaza@cst.upv.es (I. Paya-Zaforteza), ahospitaler@cst.upv.es (A. Hospitaler-Pérez).

https://doi.org/10.1016/j.jcsr.2023.108425
Received 18 October 2023; Received in revised form 12 December 2023; Accepted 14 December 2023
Available online 6 January 2024

numerical models related to composite box-girder bridges are remarkably scarce, with only two studies identified by Liu et al. [4]. This is a small number compared to the total of 46 studies reviewed on the effect of fire on bridges, encompassing both numerical modelling and experimental test analyses. Lastly, there is a complete lack of experimental studies focused on composite box-girder bridges.

Against this backdrop, this study aims to contribute to the enhancement of bridge resilience against fire hazards with a special focus on composite box-girder bridges. To achieve this objective, the effects of a real fire incident on a composite box-girder bridge located in Valencia, Spain, are examined using numerical models. A comparison is then made between the model analysis results and the actual post-fire condition of the bridge, highlighting the strengths and limitations of numerical modelling in this context. Additionally, the paper details the repair works carried out to fully restore the operational capacity of the bridge and the key lessons learnt from the incident. These findings are highly valuable for researchers, practitioners, and transportation network management authorities in their efforts to improve bridge safety and resilience.

2. Case study

The *Puente de las Flores* (or "Bridge of the Flowers" in English) is a singular structure completed in 2002 which crosses the old Turia riverbed in the city of Valencia, Spain (see Fig. 1a and b). The deck is formed by a set of longitudinal and transversal composite box-girders intersecting diagonally and defining hexagonal and triangular deck modules (see Fig. 1c). The bridge has a total length of 147.3 m and a width of 24 m. It crosses the old riverbed by means of eight spans. The span length is 18 m for the intermediate spans, 19.15 m for the end span adjacent to Abutment 1 and 20.15 m for the end span adjacent to Abutment 2 (see Fig. 1a). The distance between the axes of the main longitudinal girders is 6 m, and the maximum depth of the box-girders, which have inclined webs, is 600 mm (see Fig. 2c and d). The structural section of the bridge is completed with a concrete slab with an average thickness of 25 cm and two layers of longitudinal and transversal reinforcement. A 15 mm steel plate diaphragm is installed at the intersection of longitudinal and transversal steel girders to provide structural continuity and stiffness. Fig. 2a depicts a plan view of the structural elements in the span affected by the fire, and Fig. 2b shows a typical transverse section of the bridge. Fig. 2c, d and e illustrate the cross-sections of the longitudinal, transversal and diaphragm girders, respectively.

On December 4th, 2022 at around 5:30 am, a fire broke out beneath the bridge when several piles of pallets stored under the bridge and close to the Abutment 2 were intentionally set on fire (see Fig. 3). The pallets came from a flower replanting project conducted in November and its exact number and location was not precisely known.

Following the fire, the central lane of the bridge was closed to traffic, allowing only light vehicles and pedestrians to use the rest of the bridge. As repair works on the bridge began, this restriction was further extended to exclusively accommodate cyclists, scooters, and pedestrians. The post-fire condition of the bridge showed that spalling had occurred in the walls of Abutment 2 with a maximum depth of 3.5 cm (see Fig. 4a) and, in a more limited extension, in the triangular deck module close to Abutment 2 (see Fig. 4b) with a maximum depth in the order of 2 cm. Additionally, visual inspection also revealed an important local buckling in two segments of the bottom flange of the diaphragm girder as well as out of plane displacements in sections of both longitudinal and transversal girders (Fig. 4a, b and c). Cracks with different length also appeared in three weldings (see Fig. 4d). An elevation of the deck in the area close to the abutment was also observed (Fig. 4e).

To gain further knowledge on the state of the bridge, the following works were undertaken:

Fig. 1. Views of the "Puente de las Flores" showing also the area affected by the fire. Elevation (a), top (b) and bottom (c) views of the "Puente de las Flores".

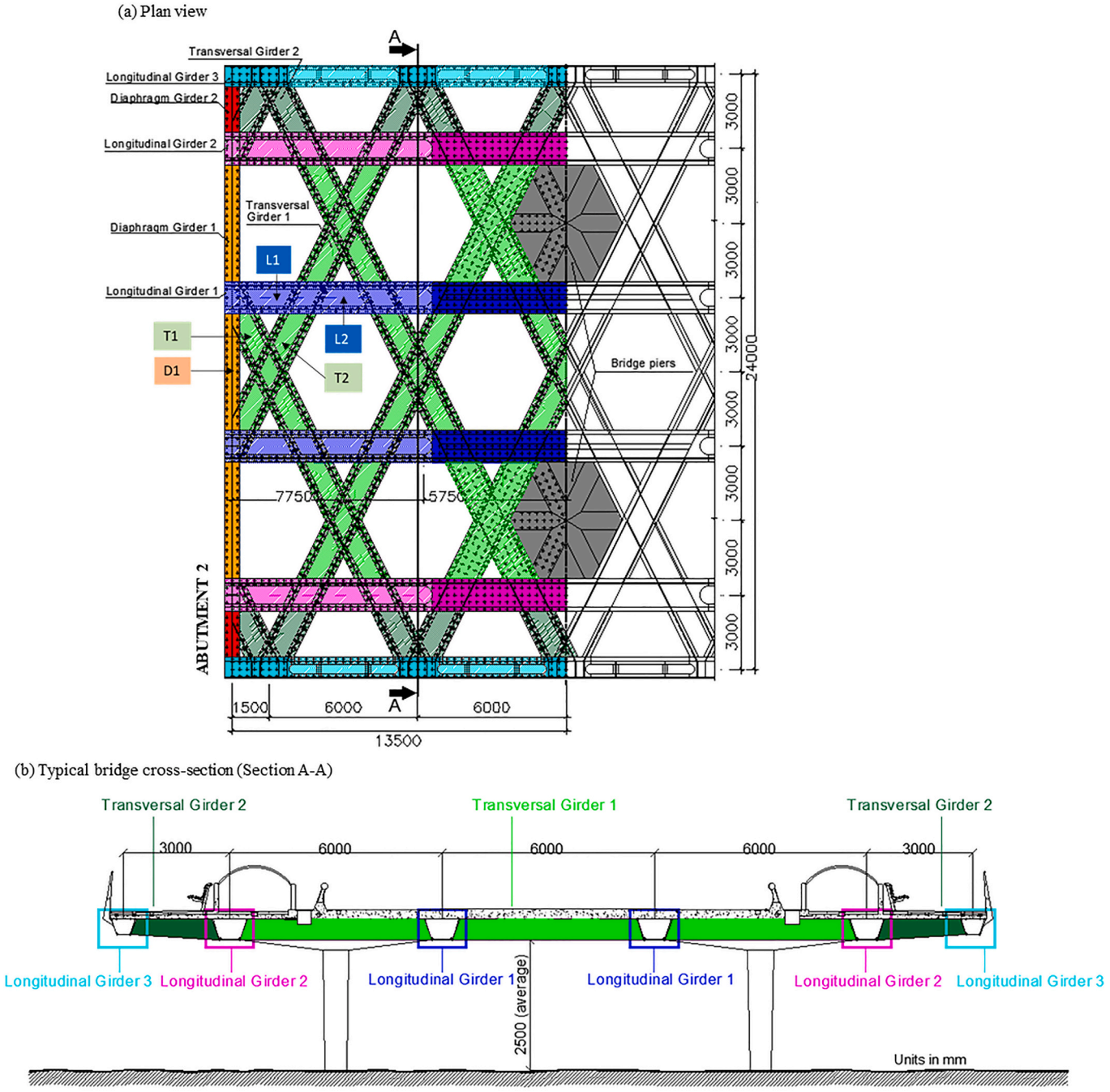

Fig. 2. (a) Plan view of the structural elements in the span affected by the fire. (b) Typical bridge cross-section with transversal girders depicted schematically (section A-A). (c) Cross-section of longitudinal girders. (d) Generic cross-section of transversal girders. (e) Cross-section of diaphragm girder. The position of the concrete slab is shown, but its thickness is variable and not drawn.

- Concrete cores were extracted from fire affected areas of the Abutment 2 and tested in compression. Compressive strength was consistently higher than the characteristic compressive strength specified in the design (25 MPa), and even surpassed the strength measured in a core drilled from a non-fire-affected area of the abutment. Concrete cores extracted from the concrete slab were reduced in length and were not considered sufficiently representative. Compressive strength was also estimated with the impact rebound hammer. Results of these tests revealed a significant variability in the compressive strength within the fire-affected areas of the abutment and, at a minimum, in the order of magnitude of the design specifications, whereas in the concrete deck results were much more homogeneous, with compressive strength values between 33 and 37 MPa.
- Tensile tests were conducted on steel specimens extracted from the diaphragm girders close to Abutment 1 (non-affected by the fire) and close to Abutment 2 (affected by the fire). Yield strength and ultimate strength were comparable and very close to the design specifications. Also ductility specifications (ratio of the ultimate tensile strength to the specified minimum yield strength, ratio of the ultimate strain to the yield strain and elongation at failure) met the requirements specified in national bridge design recommendations

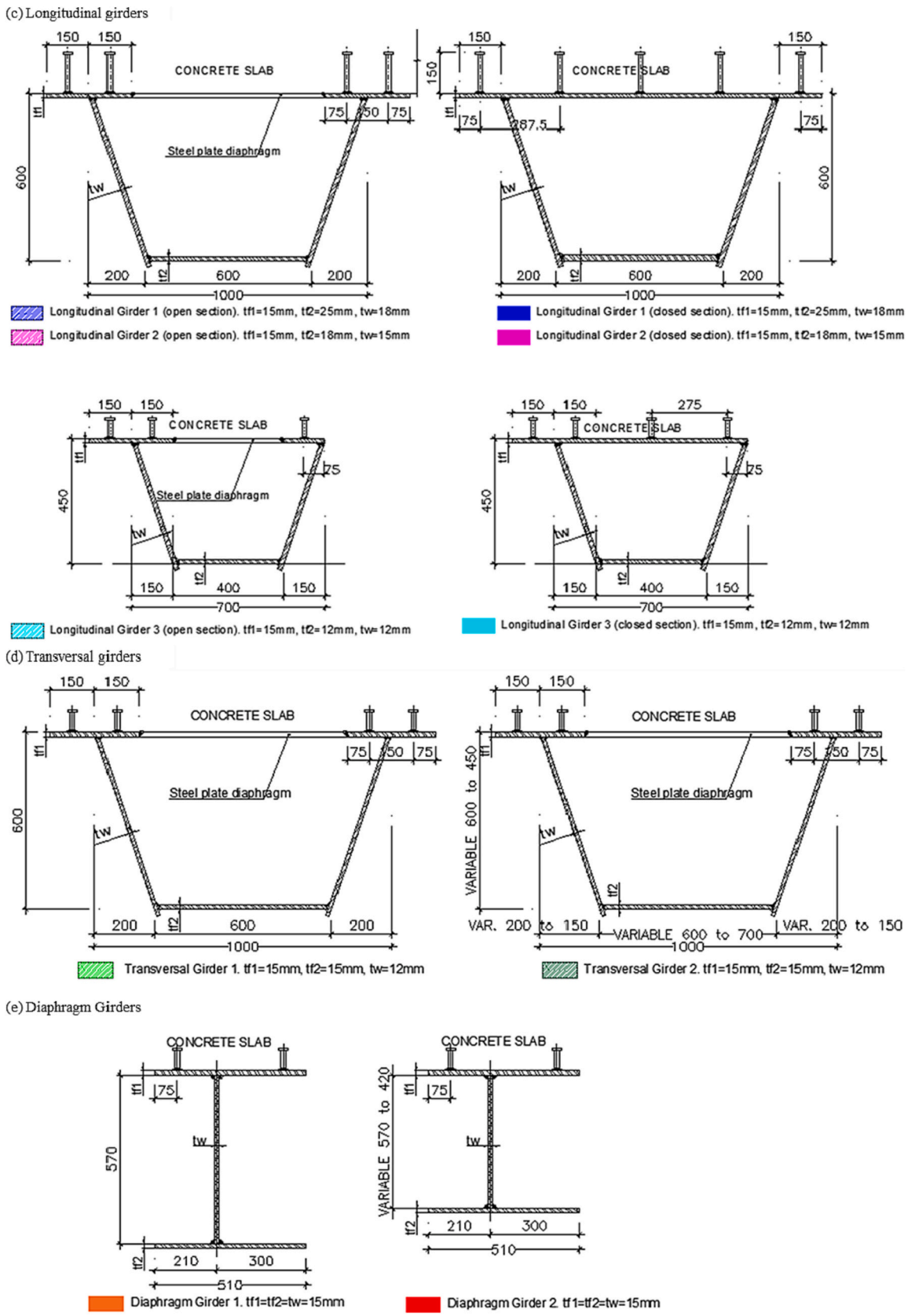

Fig. 2. (*continued*).

[20]. The acceptable strength and ductility of the steel of the girders despite the fire was further confirmed by Vickers hardness tests.

- Weldings in the fire affected area were tested using the magnetic particle testing procedure and were in satisfactory condition (except for the three cracked weldings mentioned above).

Fig. 3. Fire development under the bridge.

- A 3D scanning of the steel elements in the fire affected area was conducted and confirmed local buckling in portions of the transversal girders.
- A levelling was also undertaken to determine the relative vertical displacements of the bridge deck with respect to the Abutment 2. It revealed a vertical uplift of the central part of the deck in the area close to the Abutment 2 with a maximum value of 4.2 cm.

3. Numerical analysis of the fire event

3.1. Introduction

A three-step analysis was undertaken to assess the effects of the fire on the bridge. Firstly, a three-dimensional Computational Fluid Dynamics (CFD) analysis was conducted to determine the heat fluxes impinging the bridge structure due to the fire. Then, a finite element (FE) heat transfer analysis was conducted to calculate temperature distribution within the bridge elements over time. Finally, a non-linear 3D FE structural analysis was performed, incorporating material

Fig. 4. Post-fire visual inspection of the bridge. (a) Overall view of the most damaged area indicating maximum spalling (s_{max}) in Abutment 2 as well as the diaphragm girder main damage. (b) Concrete deck spalling and overall view of out-of-plane displacements. (c) Detail of local buckling on diaphragm girder. (d) Detail of welding crack, (e) Detail of deck uplift movement noticed by the inclination of the expansion joint.

behaviour at high temperatures, thermal-induced loads, mechanical loads, and boundary constraints. The structural response was assessed to identify areas of concern and potential structural failure.

3.2. Fire model

The first step in the numerical modelling of the event and its effects on the bridge was the creation of a three-dimensional numerical model using CFD techniques with the software Fire Dynamics Simulator (FDS). FDS was validated in the past [21,22] for bridge related fire engineering problems and provides a numerical solution for the low-speed thermal flow Navier-Stokes equations in the time domain, emphasizing the smoke and heat transport from the fire. The creation of a FDS model of the bridge fire event requires the definition of:

- A control volume defined with rectangular cells in which the fire occurs and where boundary conditions are properly defined to reflect that the fire occurred in an open environment.
- The characteristics of the fire load: location, heat release rate (HRR), fire size, fire duration, reaction type, combustion model and turbulence model.

From this input data, the results provided by the fire simulation included, among others, fire propagation, temperature distribution in the bridge environment, and heat flows that impact the structure.

3.2.1. Control volume and boundary conditions

In the event of an under-deck fire, the hexagonal-grid shape of the steel girders facilitates the creation of smoke reservoirs. This impacts the movement of smoke, the enclosure of hot gases, and the distribution of temperatures, leading to differences from what would be observed if the deck were a flat surface. Therefore, the FDS model included a detailed representation of the geometry of the bridge including both, Abutment 2 and the first bridge span (see Fig. 5). Beyond this span, boundary conditions (temperature and pressure) were assimilated to ambient conditions due to the open nature of the scenario. This approach allowed for a precise examination of the critical regions where the fire load is situated, while effectively managing the size of the fire model and the analysis time required, all without compromising the reliability of the results.

A key parameter of any FDS model is the cell size (dx) which is related to the characteristic fire diameter (D^*) since U.S Nuclear Regulatory Commission (NRC) [23] recommends a D^*/dx ratio between 16 -fine mesh and 4 – coarse mesh. D^* was obtained using Eq. (1) proposed by the NRC:

$$D^* = \left(\frac{\dot{Q}}{\rho_\infty \bullet c_\rho \bullet T_\infty \bullet \sqrt{g}} \right)^{\frac{2}{5}} \quad (1)$$

On this basis, and according to the variables detailed in Table 1, D^* equals to 3.96 m and therefore a cubic cell size (dx x dy x dz) of 0.24 m × 0.24 m × 0.24 m would be considered a fine mesh. However, it should be noted that Eq. (1) was developed to adequately resolve plume dynamics, along with other geometrical characteristics of a limited number of tested models which cannot be extrapolated to be used for all models. On this basis, and to ensure a realistic modelling of the physical phenomenon while capturing the detailed bridge geometry on the vicinity of the abutment, a 0.1 m × 0.1 m × 0.1 m was implemented in the critical region close to the fire load. Similarly, a cubic cell size (dx x dy x dz) of 0.2 m × 0.2 m × 0.2 m was implemented in the further region, which is sufficient to capture secondary phenomena occurring away from the fire location. The control volume of the 3-dimensional transient model is therefore comprised by a total 828,900 parallelepiped cells as outlined in Fig. 5c below.

3.2.2. Fire load

The fire load design considered in the CFD model was based on the information provided by València City Council and photographic evidence of the fire subproducts remaining after the fire incident (unburnt materials at ground level and visible soot along the bridge elements). Outcome from the research study confirmed that the fire location was restricted to the bridge abutment area, specifically within the area

Table 1
Input parameters for Eq. (1). Details are given in Section 3.2.2 for the heat release rate.

$\dot{Q}$ - heat release rate (KW)	ρ_∞ - air density (kg / m^3)	c_ρ - specific heat (kJ/ KgK)	T_∞ - ambient temperature (K)	g - gravity (m/s^2)
34,700	1.204	1.005	293	9.81

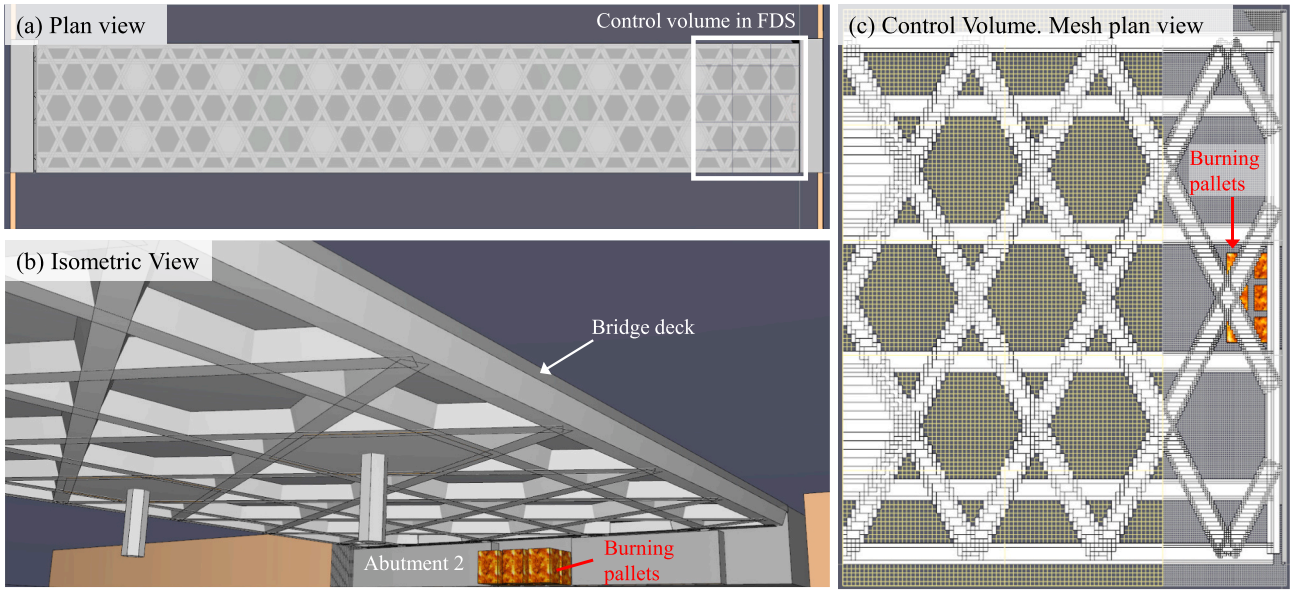

Fig. 5. (a) Plan view of the 3D model showing the control volume. (b) Isometric view of the 3D model of the case study bridge. (c) Plan view of the control volume with the finer mesh region highlighted in grey and the coarser mesh region highlighted in yellow. (For interpretation of the references to colour in this figure legend, the reader is referred to the web version of this article.)

created by the abutment recess in plan (see Fig. 5c).

Additionally, it was confirmed that the fire source comprised several piles of wood pallets of unknown height. The size of the fire load was based on the area occupied by the soot and unburnt materials at ground level, incorporating the typical dimensions of a EUR-pallet (i.e. 1.20 m × 1.00 m). Similarly, to consider the potential worst-case scenario and yet a realistic situation, each pile of pallets was assumed to contain 14 units, which is equivalent to piles of 1.7 m in height. This was considered an onerous scenario as it would be the maximum height that pallets would be comfortably stacked by manual means. Considering the above, 6 piles of 1.7 m-high pallets separated 0.3 m between them were modelled within the CFD analysis (Fig. 5). Considering all pallets burning simultaneously, a peak HRR per pile of pallets of 5.78 MW and a total HRR (six piles) of 34.7 MW was implemented for the CFD analysis. This HRR value is based on the results from fire tests carried out on wooden pallets by the NIST [24]. These tests indicated that HRR for single stacks of pallets consisting of two, four and eight pallets increases in a nearly linear form with the number of pallets, a trend also noted by Babrauskas in the SFPE Handbook [25]. Based on this, a linear extrapolation of the NIST experimental results [24] was used to obtain the HRR over time for each pallet pile as shown in red in Fig. 6.

3.2.3. Combustion model

The approach to model fire reactions in the CFD assumes a single fuel specie composed of C, H, O, and N that reacts with air to form products H_2O, CO_2, soot, and CO. On this basis, the chemical formula for wood pine in line with the SFPE Handbook [25] and the yields for soot and CO and hydrogen fraction in soot is specified.

Pyrolysis is defined though the specification of the HRR on each surface. Once HRR is specified, FDS uses the heat of combustion defined by the combustion reaction to calculate the fuel vapor mass release rate that will result in the desired energy release. The simple chemistry model is implemented within the CFD model, in which the reaction of fuel and oxygen is infinitely fast and controlled only by mixing as recommended by default by FDS.

3.2.4. Fire duration

Total duration of fire model was set to stop after 45 min from the beginning of the fire once HRR was fully developed and decay phase was stable. It should be noted that this does not correspond to the actual duration of the fire as fire brigade intervened to tackle the fire.

3.2.5. Materials and heat transfer

The boundary conditions along bridge surfaces and surrounding areas were set to model heat loss appropriately. The concrete, steel material and its associated temperature-dependent thermal properties were implemented within the CFD model in line with the recommendations of Eurocode 2. Part 1–2 [26] and Eurocode 3. Part 1–2 [27] respectively.

The control volume was extended around the bridge area by at least 1 m to account for the smoke flowing out the obstruction area and to avoid the implementation of a strict 'ambient' boundary condition (i.e. 20 °C and $1.013*10^5$ Pa) too close to the fire location which could lead to distorted results.

3.2.6. Wind conditions

Wind can tilt the flames provoked by a bridge fire, significantly modifying the heat fluxes impinging the bridge deck surfaces as detailed in [16,21,28]. However, wind was not considered in this study because, at the day and time of the incident, the Spanish Meteorological Service station in Valencia located at 1 km from the bridge recorded an average wind speed between 1.10 and 1.70 km/h (0.3 to 0.47 m/s, respectively) [29]. To contextualize these values, according to the Beaufort scale [30] - an empirical measure correlating wind speed with observed conditions at sea or on land - the recorded values correspond to the lowest end of the scale (i.e., between 0 and 1, leaning towards 0, depending on the source), equivalent to less than 2 km/h. In land conditions, a value of 0 on this scale indicates calm conditions, were smoke would rise vertically unaffected by the wind.

3.2.7. Output devices

To evaluate the temperature distribution within the bridge, a number of output devices were placed along the model as follows:

- Temperature slices were installed evenly distributed perpendicularly to global axis x, y and z.
- A total of 821 solid-phase devices capturing the adiabatic surface temperature were installed evenly distributed along all structural elements (see Fig. 7). Each structural element had at least 3 solid-phase devices to account for the temperature differences between the faces of the same structural element. The adiabatic surface temperature is the temperature used to transfer the thermal information from the CFD model to the FEM heat transfer model following

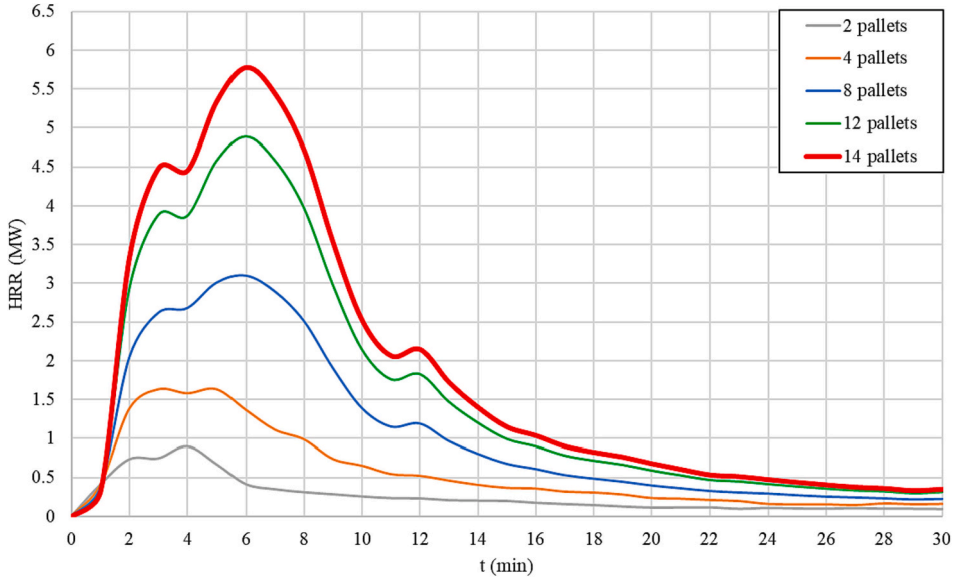

Fig. 6. Heat Release Rate of different pallet piles depending on the number of pallets. Selected pile highlighted in red (14 pallets). (For interpretation of the references to colour in this figure legend, the reader is referred to the web version of this article.)

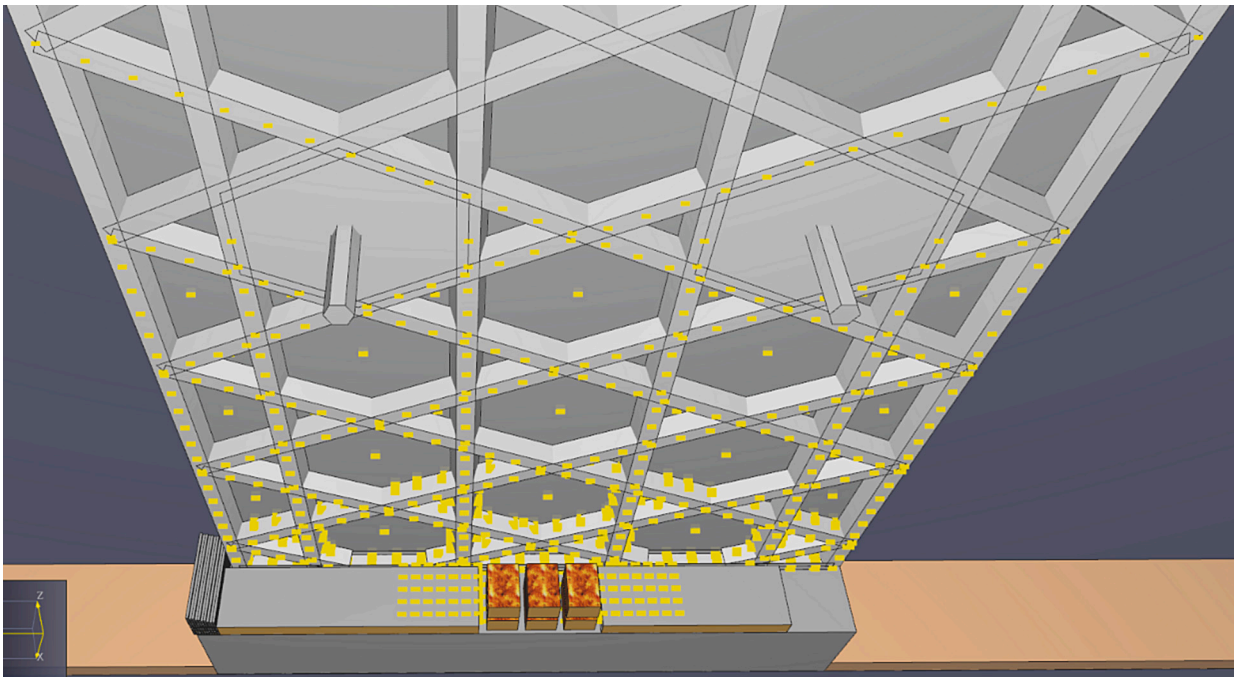

Fig. 7. Bottom view of the CFD model. Location of solid-phase devices to measure adiabatic temperatures are displayed as yellow rectangles. (For interpretation of the references to colour in this figure legend, the reader is referred to the web version of this article.)

the methodology established by Wickström [31] and validated by Alos-Moya et al. [21,22] for bridge fires.

These output devices were used to print adiabatic surface temperatures for each time step.

3.3. Fire model validation

3.3.1. Flame and smoke spread

Fig. 8 presents a visual representation of flame spread from the CFD model and can be used to qualitatively assess the agreement between the fire model results and the observed characteristics of the real fire incident, as depicted in the site photos taken after the event (see Fig. 9). Results from the CFD model are consistent with the site photos, indicating a close match between the model predictions and the actual fire incident. Clearer on-site areas correspond to locations where flames impinged on the structural elements, preventing settling of smoke soot. Conversely, darker areas correspond to locations where soot settled due to the absence of flame impingement. Additionally, the fire witnesses reported smoke spread along the bridge expansion joint during the fire

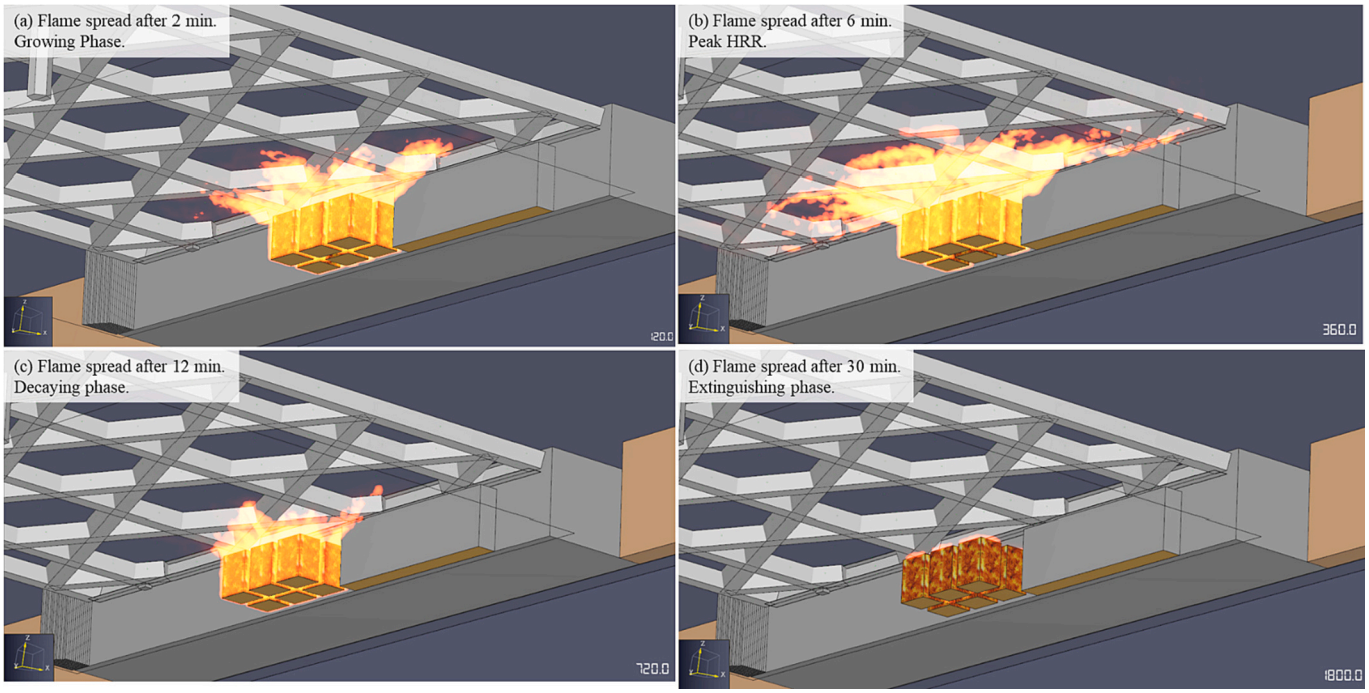

Fig. 8. Flame spread under the bridge during the fire incident: (a) growing phase, (b) peak HRR, (c) decay phase, (d) extinguishing phase.

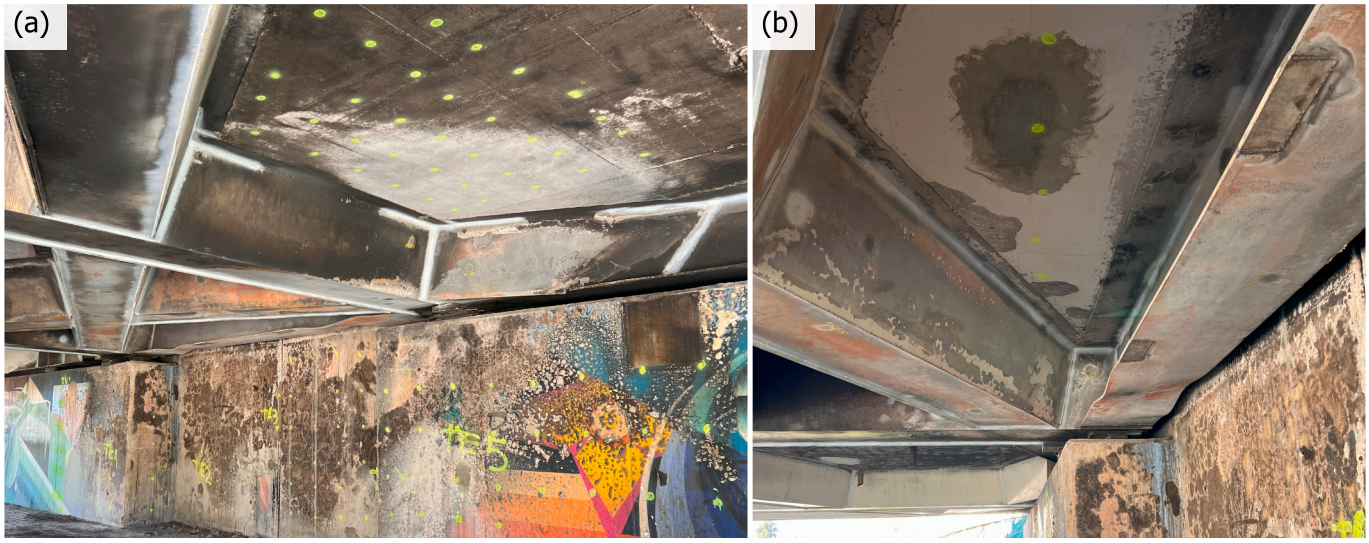

Fig. 9. View under the bridge after the fire incident. Clearer areas correspond with areas where flames impinged on to the structural elements and soot did not settle. Darker areas correspond with areas where soot settled. Grey areas in (b) correspond to areas were concrete suffered spalling or where trials were made to extract concrete cores for compressive strength testing.

incident. Fig. 10 demonstrates how the CFD model successfully captures this phenomenon, corroborating witnesses' observations. It must be noted that on-site soot settlement was nor perfectly symmetrical, so the arrangement of the pallets was probably not perfectly symmetrical as assumed in this analysis.

3.3.2. *Spalling*

There have been numerous studies attempting to identify the relevant factors causing spalling in concrete structures subjected to fire. These factors include the initial strength of concrete, moisture content, concrete density, porosity, permeability, intensity of the fire, loading conditions, type and size of aggregate, amount of reinforcement, heating rate, temperature level, thermal restraint, section shape, and section size. The coupling action of all these variables creates a risk factor for spalling to occur, which can explain the data dispersion from experimental tests and the challenges in predicting it via numerical models at a macroscopic scale.

Hua et al. [19] compiled results of concrete specimens tested under different fire curves. Elements tested under the hydrocarbon (HC), modified hydrocarbon (HCM), and Dutch Ministry of Infrastructure and Water Management (typically abbreviated as RWS) fire curves experienced spalling within 5 min from the beginning of the fire and exhibited a higher spalling rate (exceeding 2.5 mm/min) than specimens subjected to the ISO834 fire curve. The latter experienced spalling after 10–15 min of fire exposure with a spalling rate ranging from 1 to 3 mm/min. As part of their analysis, Hua et al. [19] proposed a simplified threshold of 740 °C as the spalling starting temperature for concrete elements, which is also adopted in the present study.

On this basis, Fig. 11a and b show adiabatic surface temperatures (T_{AST}) for Abutment 2 and concrete slab respectively at peak HRR as well as areas where superficial spalling was observed on site (delimited with black lines). Areas in red in Fig. 11 correspond to adiabatic surface temperatures between 750 °C and 870 °C and indicate where concrete spalling might occur. It should be noted that slab area closest to

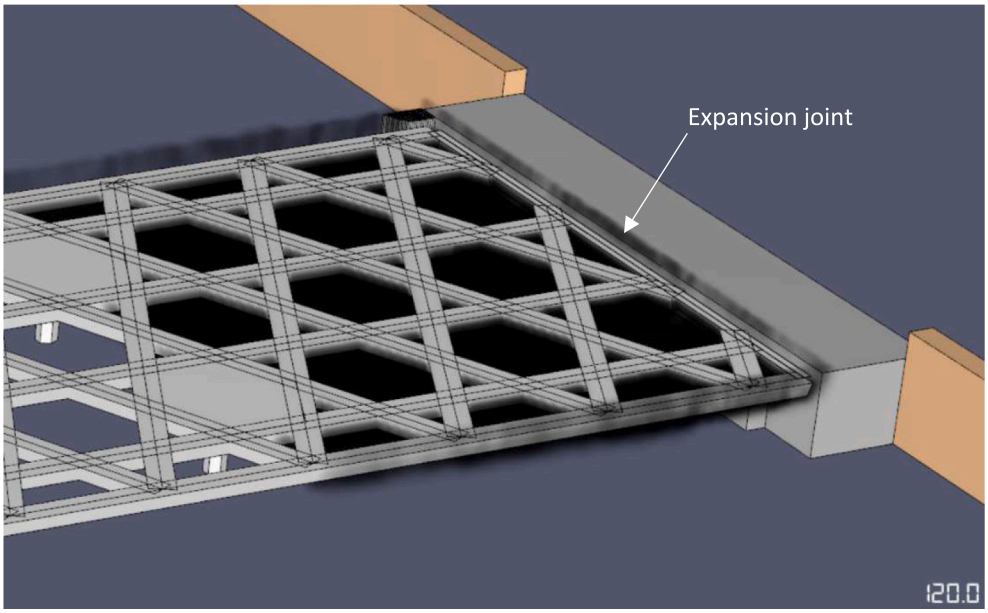

Fig. 10. Smoke leakage along the expansion joint in CFD model after 2 min.

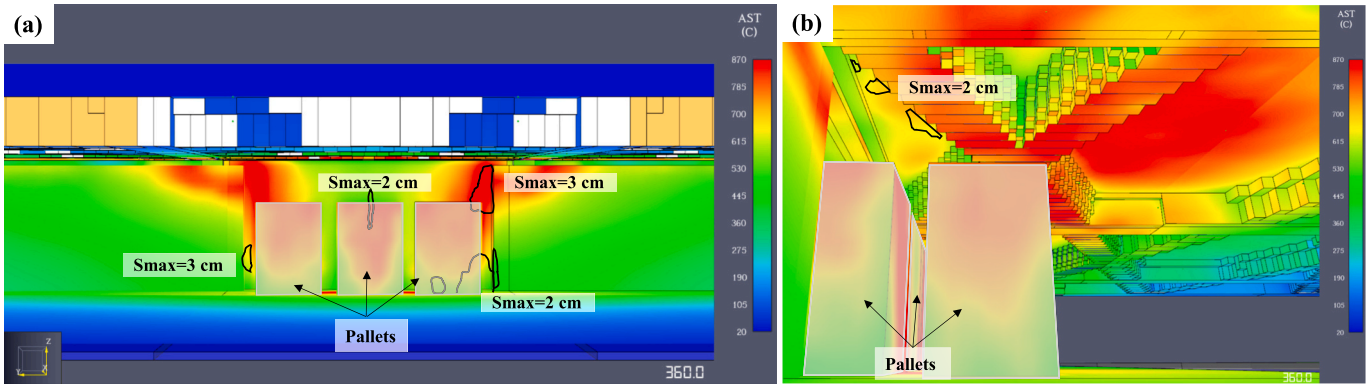

Fig. 11. Adiabatic surface temperatures after 6 min corresponding with peak HRR. Areas highlighted in red show where the adiabatic surface temperature ranges between 750 °C and 870 °C at peak HRR. Areas identified with spalling are delimited with black lines including the maximum spalling depth measured on site. (a) Abutment 2 frontal view. (b) Concrete slab. (For interpretation of the references to colour in this figure legend, the reader is referred to the web version of this article.)

Abutment 2 does not achieve the maximum peak T_{AST} at the time of peak HRR due to local underventilated conditions within the area closest to the fire location.

It can be observed that critical areas outlined by the CFD results are related with those areas where spalling was identified on site (i.e. central and lateral areas along the abutment recess) and closest surface slab to the fire location. Note that actual concrete surface temperatures will be lower than the adiabatic surface temperatures obtained with the CFD model and define a better approach to evaluate spalling. Since obtaining concrete surface temperatures requires heat transfer models and such models are presented in Section 3.4, a more detailed discussion of predicted spalling versus actual spalling is provided there.

3.4. Heat transfer analysis

Fire models traditionally focus on predicting heat flux to geometrically simple solid surfaces, which are thermally defined by one-dimensional heat transfer models. Conversely, thermal finite element models typically assume a global gas temperature surrounding a detailed two or three-dimensional element. In this study, the nonlinear finite element analysis software SAFIR [32], which was developed to study structures under fire, is used to solve heat transfer. To incorporate gas phase data from numerical fire simulations (FDS calculations) into SAFIR [32] as boundary input, the concept of adiabatic surface temperature (T_{AST}), as proposed by Wickström [31] is used. Comprehensive information on utilizing T_{AST} for bridge fires can be found in Alos-Moya et al. [22] and Peris-Sayol et al. [28].

SAFIR [32] algorithm for thermal analysis relies on the computation of enthalpy rather than specific heat. This choice enhances the software's stability, particularly in cases where the specific heat curve exhibits sudden and severe variations, such as in concrete due to the evaporation of moisture. Given that the case study bridge employs composite box-girders for the deck, it becomes imperative to address heat transfer within the cavities defined by these box-girders. SAFIR [32] accomplishes this by implementing a linear convection mechanism between the internal surfaces of the cavity and the air within it. Additionally, the software computes radiation between the internal surfaces of the cavity, adhering to the following hypotheses:

- There is no heat transfer by conduction within the gas that is in the cavity.
- The specific heat of the gas in the cavity is neglected.
- The gas in the cavity is transparent to radiation (non-participating media).

The materials and its associated thermal properties have been implemented within the heat transfer analysis in line with the recommendations of EN 1992-1-2 [26] for concrete, and EN 1993-1-2 [27] for carbon steel as follows:

- Coefficients of convection on the heated surface and the one on unheated surface equal to 35 W/m^{2}K and 4 W/m^{2}K respectively as recommended by EN 1991–1-2 [33] for a natural fire. The total emissivity has been taken as 0.7.
- Moisture content of 1.5% of concrete weight.
- Concrete specific heat at ambient temperature equal to 900 J/kg K and temperature dependent according to [26]. Concrete density at ambient temperature equal to 2500 kg/m^3 and temperature dependent following [26].
- Concrete thermal conductivity implemented with its lower limit and temperature dependent in line with [26]. During cooling, there is no recondensation of the water and the thermal conductivity is considered as not reversible and considered at the value of the maximum temperature reached.
- Thermal properties for structural steel follow the equations of Eurocode EN 1993-1-2 with a density of 7850 kg/m^3.
- Steel reinforcing bars are not considered for the thermal analysis in line with Section 4.3.2 of EN 1992-1-2 [26].

Fig. 12 depicts the thermal model of a typical longitudinal girder section (section L1 in Fig. 2). It illustrates both the mesh (a non-structured quadrangular mesh with sides not exceeding 5 cm) and the thermal boundary conditions. Each number in Fig. 12 is associated with a different colour, representing a distinct temperature-time fire curve obtained from the CFD model (Dirichlet boundary condition). The temperature on the unexposed side of the concrete slab is fixed and set equal to the ambient temperature (i.e., 20 °C).

Results from the thermal analysis are outlined in Sections 3.4.1, 3.4.2 and 3.4.3 below, capturing temperature profiles at different cross-sections of composite beams and concrete elements (slab and Abutment 2).

3.4.1. Temperatures in the elevation of Abutment 2

Fig. 13a depicts the locations of representative points in the concrete of Abutment 2. Fig. 13b to 13d illustrate the evolution of concrete temperatures (T) at these points as a function of depth (d) from the exposed concrete surface and time (t). The temperatures exhibit symmetry along both sides of the abutment. Based on the results, the following observations can be made:

a) The highest temperatures occur in the area along the abutment recess close to the corner, in the upper zone (A2). This temperature reaches

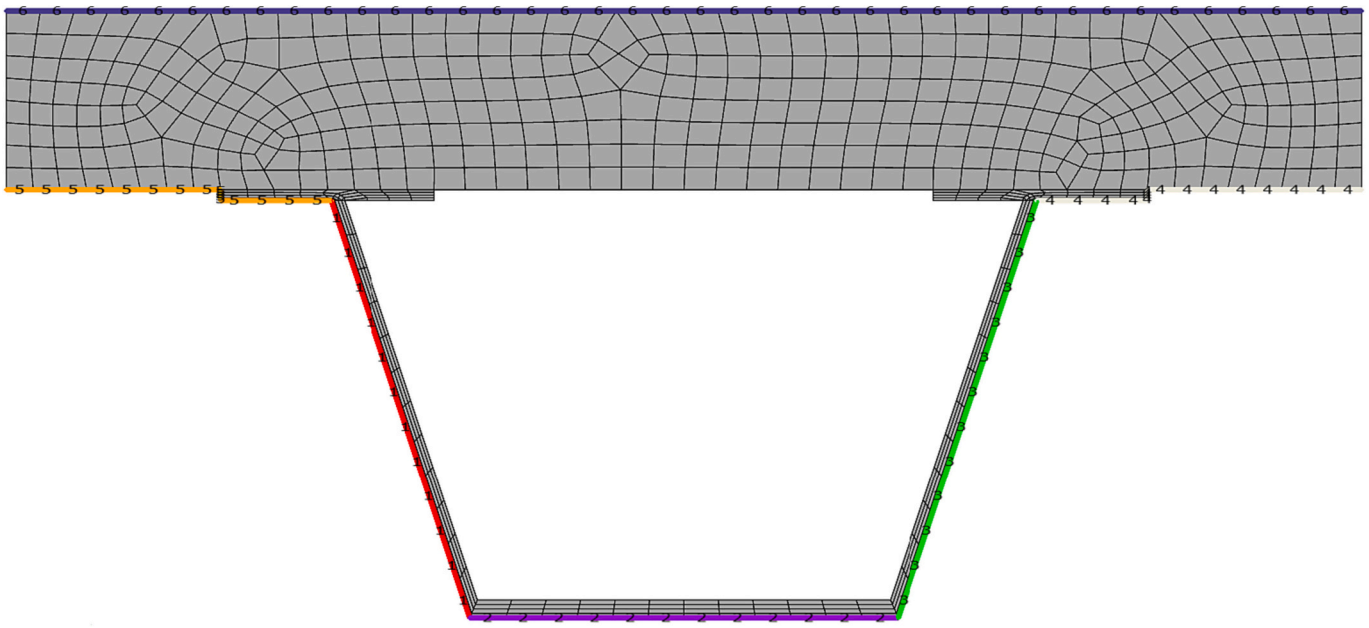

Fig. 12. Section L1 of Longitudinal Girder 1. Typical mesh and boundary conditions implemented for the FEM Heat Transfer Analysis.

a maximum value of 805 °C after 12 min. The next zone is the center-lateral zone along the abutment recess (A1) with a maximum value of 770 °C after 13 min, followed by the lateral zone (A3), reaching a maximum value of 750 °C after 14 min. Finally, the farthest upper lateral zone (A4) reaches a maximum value of 542 °C after 8 min. These temperatures are significantly higher than those measured in the concrete slab (detailed in Section 3.4.2), which explains the more pronounced spalling in these areas compared to the limited spalling in the slab.

b) Fig. 13b to 13d also show a horizontal line representing a constant temperature of 500 °C. It should be noted that this temperature marks the threshold from where concrete (excluding steel rebars) is assumed to lose its structural capacity in the Isotherm 500 method outlined in EN 1992-1-2 [26]. Although the method assumes that structural elements are subject to the ISO834 standard fire curve or similar heating regimes, this threshold can be used for qualitative estimations since both, ISO 834 and the fire under the case study bridge are cellulosic fires. The 500 °C threshold is only exceeded within the first 6 mm (worst-case scenario, A2) from the exposed abutment surface, which means that the reduced section (i.e. section excluding those concrete areas exceeding 500 °C) practically coincides with the original section when following the Isotherm 500 method for a qualitative analysis.

c) Since the concrete cover of the steel rebars (as prescribed in the project drawings) is 35 mm, the maximum temperature reached by the abutment reinforcement is around 198 °C. This temperature is much lower than the temperature at which the reinforcement starts losing strength (300 °C for cold-deformed steel and 400 °C for hot-rolled steel), indicating that the reinforcement has not suffered any loss of strength.

d) The peak concrete surface temperatures in the vicinity of the pot-type bearing supports reached a maximum value of approximately 600 °C, posing a significant threat to the integrity of these key elements. Considering this, the decision was made to replace the pot bearings.

3.4.2. *Temperatures in the concrete slab*

Fig. 14 shows the evolution of temperatures in the concrete slab at representative surfaces S1, S2, S3, S4 and S5 located in Fig. 14a. It should be noted that a homogeneous temperature is assumed for each slab surface created between steel girders. For each selected surface, figures display temperatures in the concrete (T) as a function of depth (d) from the exposed concrete surface. Based on the results, the following observations can be made:

- FDS analysis showed that maximum T_{AST} is punctually reached along S5 surface. However, higher temperatures remain longer within the closest surfaces to the fire location due to the smoke reservoir created by the steel beams and concrete slab. This configuration delays the hot gases movement away from the area and explains the spalling along surface S1 in lieu of S5. The highest surface temperatures occur in section S1, located immediately above the position of the pallets. This temperature reaches a maximum value of 636 °C after 14 min. The next most affected sections are S5 and S3, where the maximum temperatures are 516 °C and 594 °C, respectively. In the remaining sections (S2 and S4), the maximum temperatures remain below 400 °C. This explains the limited extent of spalling in the concrete slab (temperatures never exceed the mean onset value of 740 °C for spalling proposed by Hua et al. [19]) and why it appears only in section S1.

Based on the above findings and considering that both, ISO 834 and the analyzed fire are cellulosic fires, the following comments can be made:

a) Temperatures have significantly exceeded 500 °C only in the concrete section S1. However, the slab thickness at which this temperature was exceeded is minimal, approximately 5 mm. Therefore, the reduced section practically coincides with the original section and concrete damage is minimal. This is supported by the positive results obtained by the indirect measurement of slab compressive strength using the impact rebound hammer.

b) Since the concrete cover of the steel rebars (as prescribed in the project drawings) is 35 mm, the maximum temperature reached by the slab reinforcement is around 174 °C. This temperature is much lower than the temperature at which the reinforcement starts losing strength (300 °C for cold-deformed steel and 400 °C for hot-rolled steel), indicating that the reinforcement has not suffered any loss of strength.

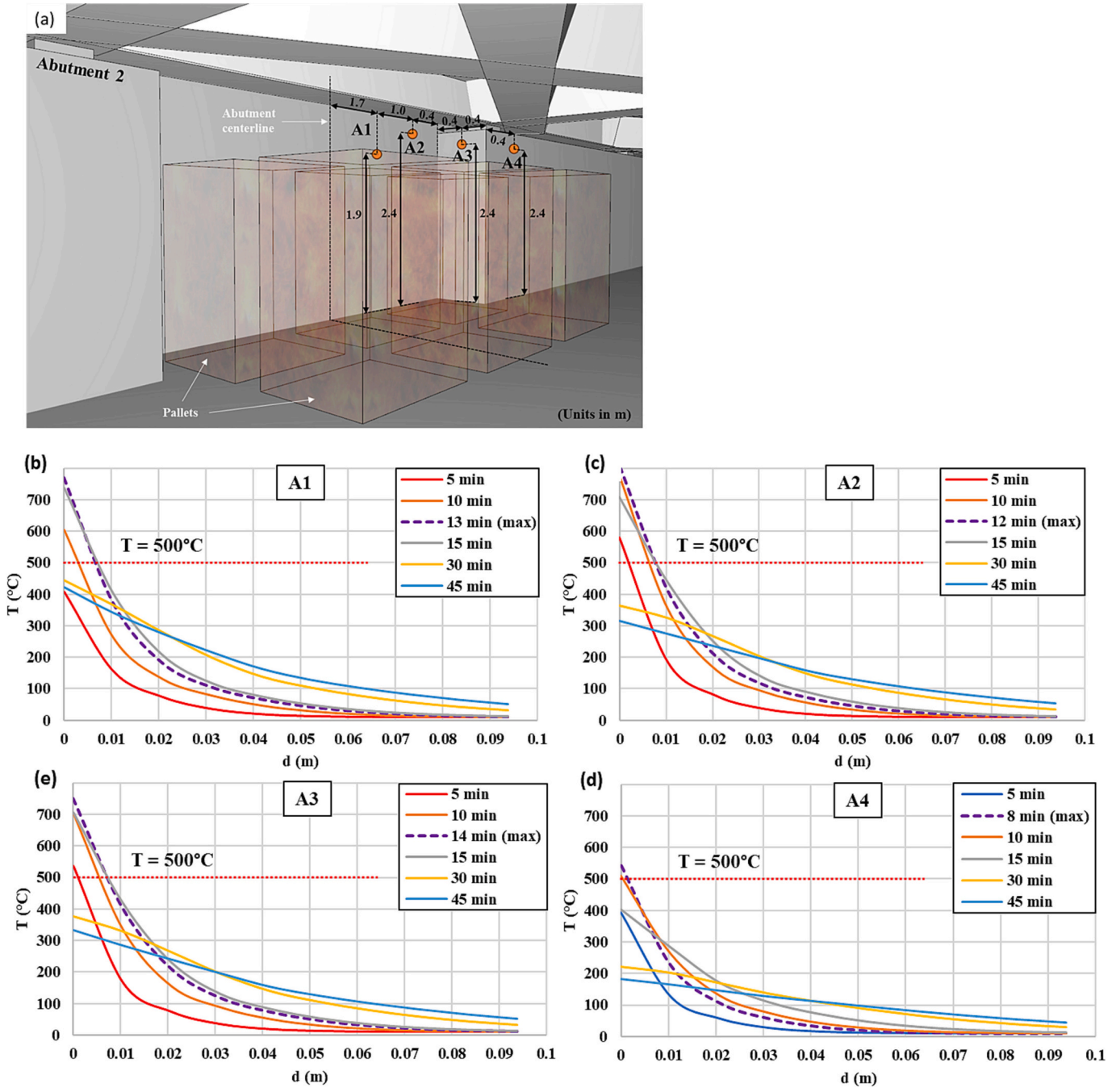

Fig. 13. Temperature evolution within the abutment in the vicinity of the fire.

In light of the above, it can be concluded that the resistant capacity of the deck slab sections remained practically unaffected by the thermal effects of the fire.

3.4.3. *Temperatures in the steel girders*

Fig. 15a shows the evolution of temperatures in a section of Diaphragm Girder 1 located just above the fire area (section named D1 in Fig. 2a) and Fig. 15b shows the distribution of temperatures within the cross section. The maximum temperature reached is 712 °C, which occurs after approximately after 17 min in the bottom-left corner (Node bf3). At this temperature, and in accordance with Eurocode EN 1993-1-2, the yield strength, the proportional limit, and the modulus of elasticity have been reduced to 23%, 7.5%, and 13% of their respective values at ambient temperature. This reduction in strength and stiffness, combined with the indirect stresses due to the structural restraint imposed on the beam expansion, explains the local buckling of the bottom flange at two segments of the diaphragm girder (see Fig. 4a and c). Buckling of the top flange does not occur because it is restrained by its connection to the concrete slab. Results also show that maximum steel temperatures always remain below 723 °C, a critical temperature at which a phase change occurs in the steel, causing embrittlement if the cooling does not occur slowly enough. The positive results obtained in the tensile tests conducted on steel specimens extracted from the diaphragm girder are explained by the temperatures not exceeding this limit. Temperatures in adjacent diaphragm girder sections are not shown as they are much lower (maximum values around 325 °C) and even below 400 °C, the temperature at which the yield strength of steel starts decreasing.

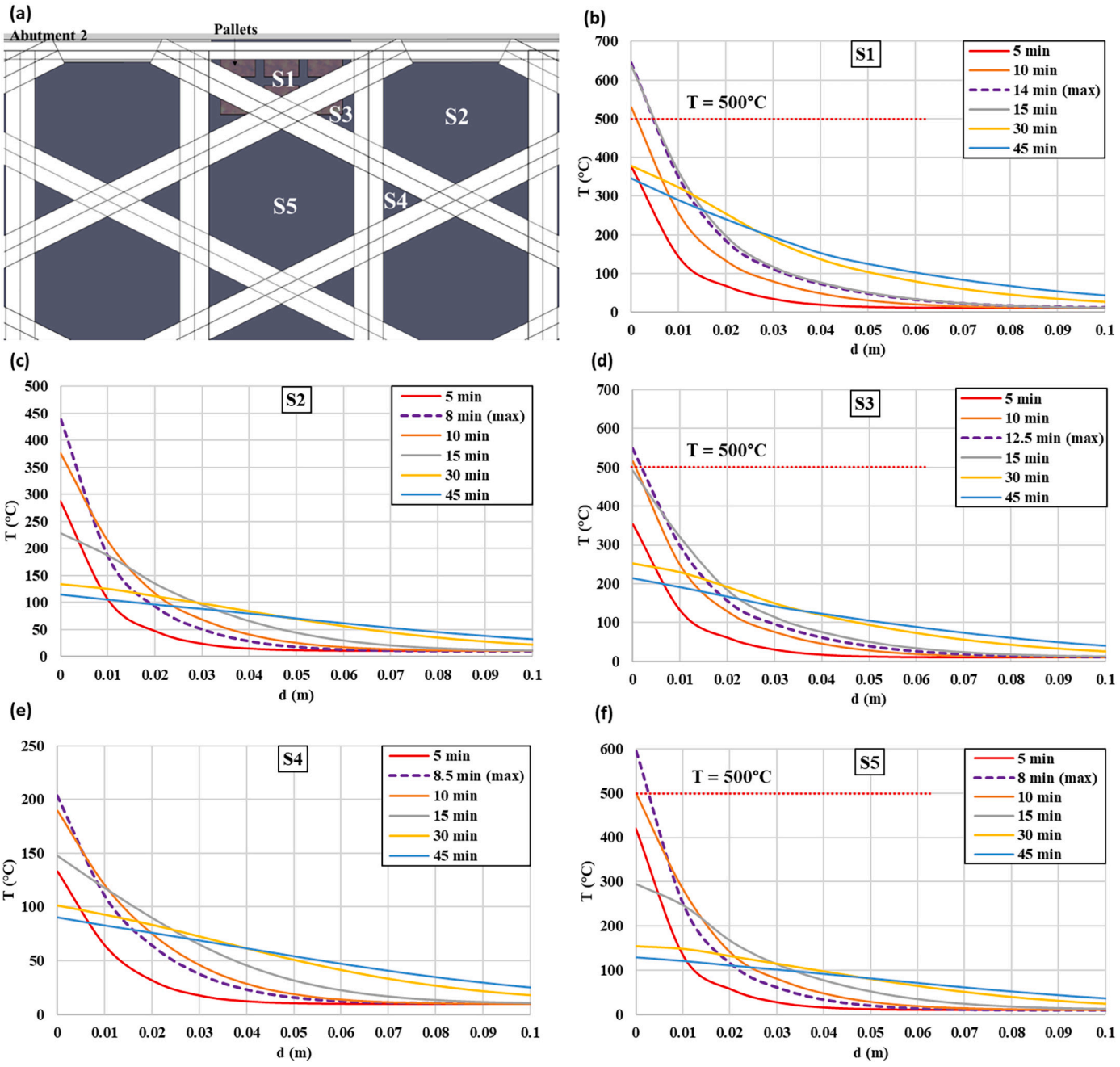

Fig. 14. Temperature evolution within the concrete slab in the vicinity of the fire.

Fig. 16a and c display the temperature evolution in two sections of the transversal girders (sections T1 and T2, in Fig. 2a) located in the vicinity of the fire load. Peak temperatures of 650 °C (bottom flange of Section T1) and 520 °C (most exposed web of Section T2) are observed. At these elevated temperatures, the modulus of elasticity of the steel is significantly reduced (35% at 650 °C and 54% at 520 °C of their respective values at ambient temperature) as well as the proportional limit (reduced to 12.5% at 650 °C and 54% at 520 °C of the values at ambient temperature). This material degradation, combined with the thermal induced actions, explain the buckling observed along the web and bottom flange of the transverse girders. This phenomenon is enhanced by the reduced thickness of the web and flange of the transverse girders (12 mm and 15 mm respectively) compared to the main longitudinal girders (18 mm and 25 mm, respectively).

Finally, Fig. 16e and g show the evolution of the temperatures in sections L1 and L2 of Longitudinal Girder 1, with section L1 being the closest to Abutment 2 and L2 being the furthest (see Fig. 2 for sections location). The maximum temperature reached is 425 °C and occurs in the most exposed web of Section L1. In the other section (L2), the maximum temperatures are around 250 °C (Section L2-w1). On this basis, it is expected that displacements of the longitudinal girder webs are much smaller than those of the transversal girder webs, as when the maximum temperatures were reached, the yield strength, the proportional limit, and the modulus of elasticity were 94.5%, 40.5%, and 67.5% of their values at ambient temperature (significantly lower reduction), and, as mentioned above, longitudinal girders are designed with higher web and flange thickness plates.

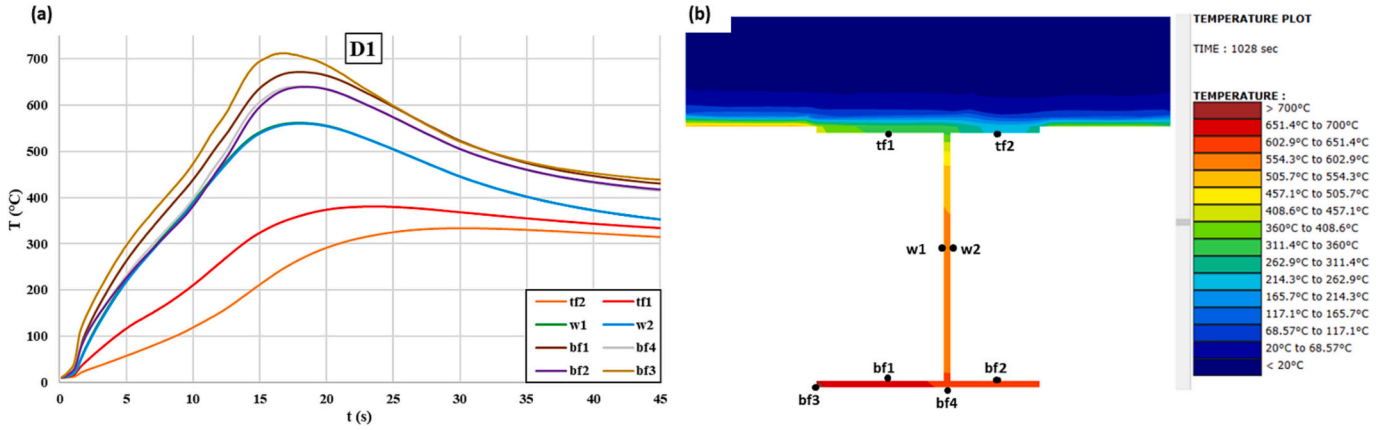

Fig. 15. Temperatures in section D1 of diaphragm girder 1. (a) Time evolution. (b) Distribution within the girder cross section after 17 min.

3.5. Mechanical response analysis

3.5.1. Methodology

3.5.1.1. General characteristics of the structural model. The structural response of the bridge during the fire has been carried out with SAFIR. SAFIR is specifically designed for modelling the behaviour of building structures during fire incidents. It transfers temperatures from heat transfer to mechanical analysis, considering the impact of thermal gradients and fire-induced forces on the structure. The mechanical analyses account for material and geometric non-linearities, as well as large displacements. Only self-weight loads are implemented within the structural analysis to facilitate the model calibration.

Fiber-type beam elements were employed for modelling beam elements, while shell finite elements were utilized for the slabs [34]. The steel reinforcements are smeared laterally, and their contribution is considered by a uniaxial model. Only an elongation in the direction of their axis will produce a stress, whereas an elongation perpendicular to the axis or a shear strain in the element do not produce any stress in the bars. The decision to employ beam finite elements for the girders in the model was motivated by considerations of numerical complexity and computational costs, given the inclusion of numerous steel members in the FEM model. It is acknowledged that this choice involves an approximation and that beam elements do not explicitly account for local buckling. However, it is crucial to emphasize that the simulation did not aim to specifically address local buckling but rather focused on elucidating the root causes of the observed on-site phenomenon and inform the repair decisions.

It is important to note that shear connection plays a crucial role in determining the ultimate capacity of composite structures at elevated temperatures, as emphasized in experimental studies by Wang et al. [35] and Pfenning et al. [36]. However, during a fire, shear studs experience slower temperature increases than steel beams due to their embedment in concrete. Research projects such as FRACOF [37], FICEB [38], MACS+ [39] and the work by Drury [40] at Lehigh University comparing numerical and experimental results support the assumption of a "rigid" shear interface in finite element models. The analysis presented in this paper adopts a similar approach, assuming that the nodes of these different types of elements (i.e. beam and shell) are defined in a common reference plane. The reference plane coincides with the mid-surface of the concrete slab element. Its location is fixed throughout the analysis and assumes a rigid behaviour between the steel beams and the concrete slab. This assumption underwent validation following the provisions of EN 1994-1-1 [46] and EN 1994-1-2 [41], which indicated a minimal reduction (less than 3%) in shear stress capacity for the worst-case scenario. This small reduction aligns with results obtained using the correlation proposed by Mirza et al. [42], indicating a maximum reduction of 6.7% in shear stress capacity. The calculated reductions affirm that potential shear connection damage was negligible, ensuring the effective collaboration of the concrete slab and steel girders as an integrated system. Consequently, the behaviour of the connectors was deemed non-critical for the overall structural integrity of the bridge.

3.5.1.2. Mechanical properties of materials. Mechanical properties of material implemented within the structural analysis was based on the construction package documentation. The steel reinforcement utilized for this project corresponds to hot rolled Class A reinforcement with a characteristic yield strength of 500 MPa, exhibiting a stress-strain curve that initiates its descent at a strain of 0.05. Similarly, the structural steel employed is a normalized non-alloy steel characterized by a characteristic yield strength of 355 MPa and designated as S355 J2G3Z35 within the construction package documentation. In addition to the steel, the concrete used in this project features siliceous aggregates and possesses a characteristic compressive strength obtained with cylindrical specimens of 30 MPa, along with a tensile strength of 3 MPa. Furthermore, the concrete has a strain at peak stress of 0.0025, dilatancy parameters of 0.25, compressive ductility parameter of 0.19, compressive damage at peak stress of 0.30, and a tensile ductility parameter of 2000 N/m^2, accounting for tension stiffening.

For the concrete slab, an average thickness of 25 cm has been considered, with two-way reinforcement implemented on both faces. The reinforcement comprises 20 mm diameter steel bars spaced at 20 cm intervals, maintaining a consistent geometric cover of 35 mm throughout the entire slab.

The shell elements employ an elevated temperature plastic-damage model with explicit transient creep, as proposed by Gernay et al. [43], for modelling the concrete. The variation of mechanical properties of concrete and steel (reinforcing and structural) at high temperatures follows the Eurocode recommendations [26,27,41].

The structural analysis uses characteristic values of the materials strength in lieu of the strengths obtained from the in-situ tests based on the following:

- The drilling machine used to extract the concrete cores from the deck slab had to be placed on the bridge pavement. The machine drilled from the top face of the slab towards its bottom face but, due to the dense grid of reinforcing bars, it was not possible to obtain cores representative of the full slab thickness, including potential fire-affected areas.
- As detailed in Section 2, results of the tensile test of steel specimens extracted from the diaphragm girders were very close to their theoretical characteristic values according to the design specifications and met the requirements of national bridge design recommendations [20].

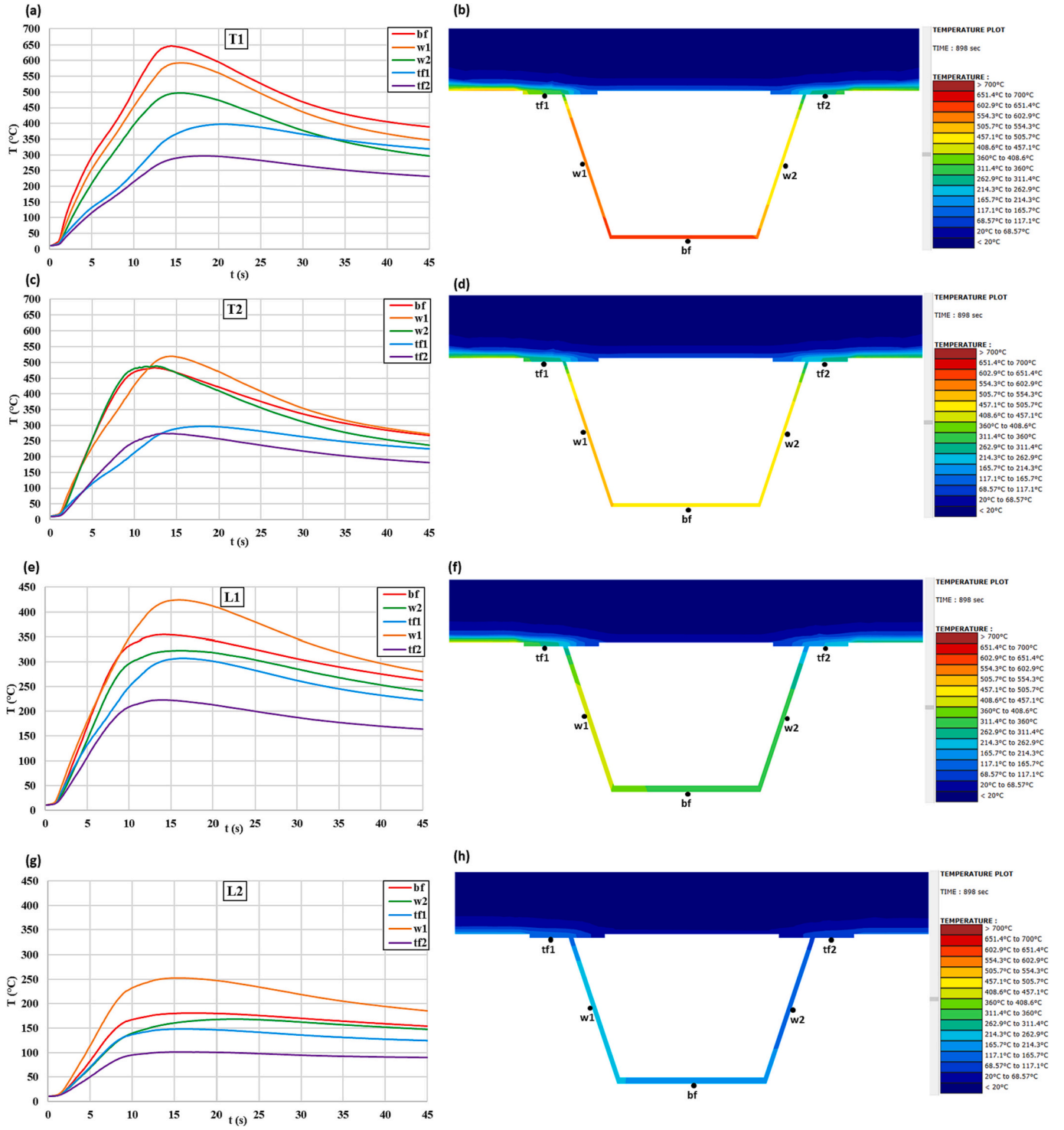

Fig. 16. Temperatures in sections T1, T2 of transversal girders 1 and 2 and in sections L1 and L2 of longitudinal girders 1 and 2. Images on the left show evolution of temperatures with time whereas images on the right show cross section temperatures after 15 min. Sections location is shown in Fig. 2.

- The partial safety factor for the relevant material mechanical properties for the fire situation, $\gamma_{M,fi}$, is taken as 1 in accordance with the Eurocodes [26,27,41].

Therefore, the use of characteristic values was a pragmatic approach given the constraints and urgency of the works, enabling swift actions to address the assessment of the bridge condition.

3.5.1.3. Boundary conditions and applied loads. The following aspects have been considered for the non-linear structural analysis (see Fig. 17):

- Connection between composite deck and Abutment 2. This connection has been modelled with non-linear springs located at each bridge bearing. These springs transfer a vertical reaction force when compressed, but they do not react when stretched (i.e., when the deck separates from the abutment), and have a very high stiffness to fully restrict vertical movement when compressed. No additional restraints have been applied to the remaining degrees of freedom.

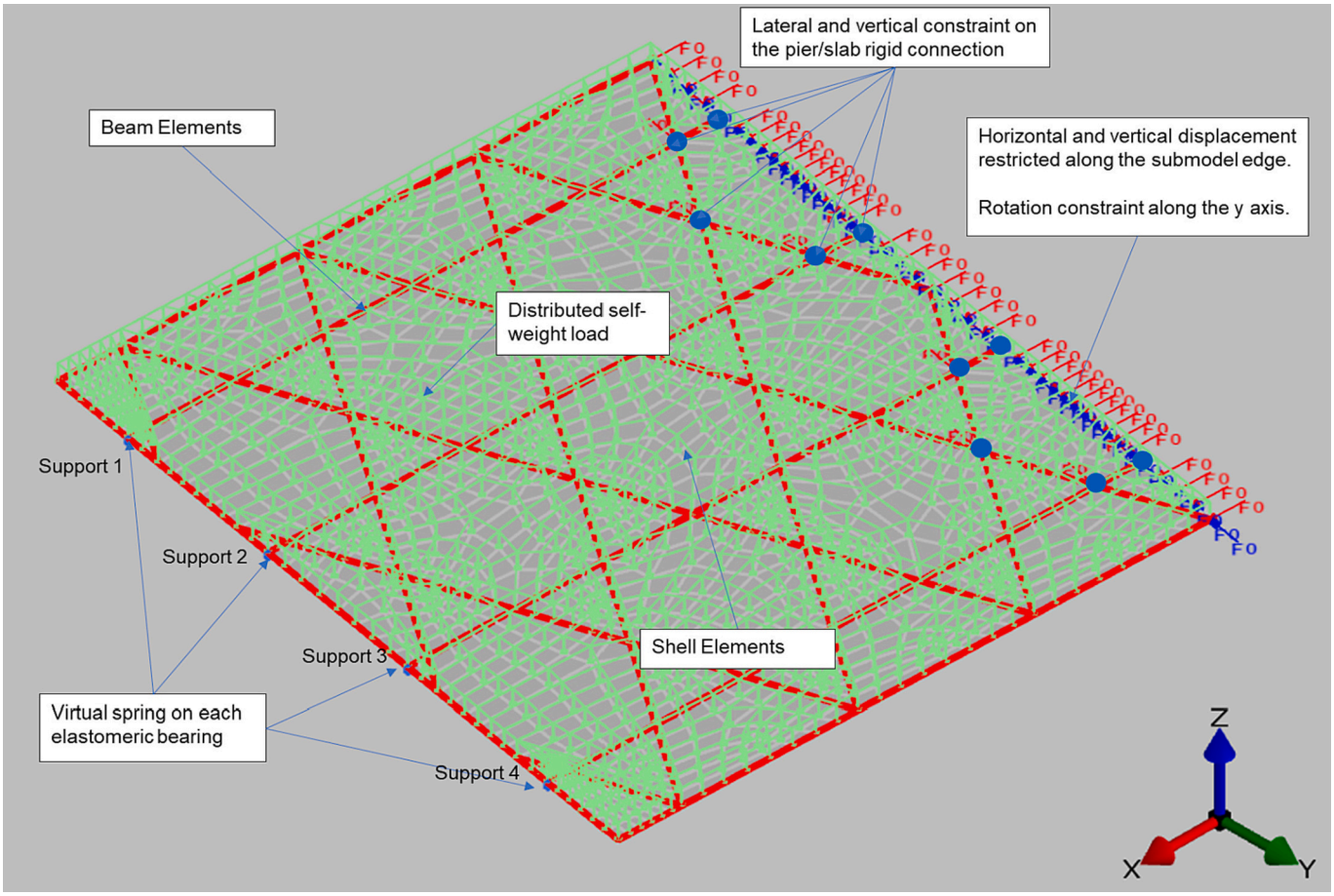

Fig. 17. Mechanical model. Beam elements (red lines), mechanical load (green arrows), shell elements (grey areas), elastomeric bearing supports (labelled blue springs supports), mechanical rigid constraints (red F0 arrows for displacement constraints and blue F0 arrows for rotational constraints). (For interpretation of the references to colour in this figure legend, the reader is referred to the web version of this article.)

This aligns with reality because: (1) the maximum longitudinal displacement of the bridge towards the abutment in the structural model is 1.5 cm, which is less than the expansion joint width, and (2) the deck is supported by pot bearings.

- Section of the bridge included in the structural model. The structural model includes only the span adjacent to the Abutment 2. To consider the influence of the rest of the structure the boundary conditions displayed in Fig. 17 have been implemented. More specifically:
  - o Vertical and lateral displacements are restrained at the nodes of connection between the piers and the longitudinal girders. This is justified because the connection between the piers and the concrete slab is very rigid and behaves as a rigid solid during the structural analysis.
  - o Vertical and longitudinal displacement is restrained along the edge at the end of the substructure. Rotation constraint along the *y* axis is also restrained throughout.

These simplifications enable to avoid numerical instabilities and significantly reduce the model computational cost. The analysis considers only self-weight to facilitate the structural model calibration (see Section 3.5.1.4). No live loads where applied because the ability of the bridge to sustain live loads at ambient temperature was verified with a specific model built with Sofistik [44] and a load test. Details of this model can be found in [45].

3.5.1.4. Validation of the model at ambient temperature. To check the validity of the simplifications described in Section 3.5.1.3, reactions at ambient temperature due to self-weight at the abutment supports obtained with the SAFIR model were compared to those obtained with a 3D model of the full bridge built with the software Sofistik [44] (see Table 2). Differences are considered acceptable given that: 1) Sofistik model was built with shell elements that perfectly match the geometry of the deck, whereas the SAFIR model used a combination of beam and shell elements which does not perfectly replicate the deck geometry, 2) the goal of the SAFIR structural model was to qualitatively assess the response of the structure to fire.

The absence of a direct comparison between the numerical model displacement results and in-situ laser scanning measurements stems from the limitations of the employed model and the data and time available for the analyses. The numerical model used cannot accurately reproduce the small transverse displacements measured by laser scanning. To achieve this, a more refined and time costly shell element model is necessary, along with the incorporation of pre-existing imperfections which were unknown. While time constraints prevented the

Table 2
Support reactions at Abutment 2 for the full structural model and proposed structural submodel at ambient temperature.

Support	Vertical Reaction – Full Structural Model (kN)	Vertical Reaction – Proposed Structural Submodel (kN)	Variation (%)
Supports 1 & 4	490	410	16.3%
Supports 2 & 3	290	314	7.6%

development of a full shell element model for this study, its consideration has been earmarked for future work, recognizing the importance of capturing fine-grained structural details and improving the precision of displacement predictions in subsequent research endeavours.

3.5.2. Results

The figures below outline the vertical displacements (Fig. 18) and axial loads (Fig. 19) during the fire scenario.

The following conclusions can be extracted from the results above:

- The bridge structure remains stable 25 min after the start of the fire, showing no signs of collapse during the incident.
- The numerical model is unable to reproduce the concrete deck uplift observed on site along its central part next to Abutment 2 (see Fig. 4e). Furthermore, in the numerical model, the central area near the abutment experiences vertical deflections in the direction of gravity with a maximum value of 11 mm. It should be noted that results from other numerical models of fire simulations in bridges (see e.g., Alós-Moya et al., 2014 [22]) show an uplift when the deck, due to its thermal expansion, impacts the abutment. However, this collision did not occur in this case. This was not observed on site during the postfire inspections, and the numerical model predicts an expansion of 1.5 cm, much smaller than the expansion joint width.
- Maximum vertical deflection is reached along the concrete slab area labelled as S5 in Fig. 14a. This maximum deflection achieves 83 mm after 12 min from the beginning of the fire. After this point, as fire load is within the decay phase, vertical deflection starts reducing until the end of the simulation (refer to node 924 of Fig. 18e and f). The maximum vertical uplift occurs at the extreme nodes along the diaphragm girder. This uplift reaches a peak value of 70 mm at 12

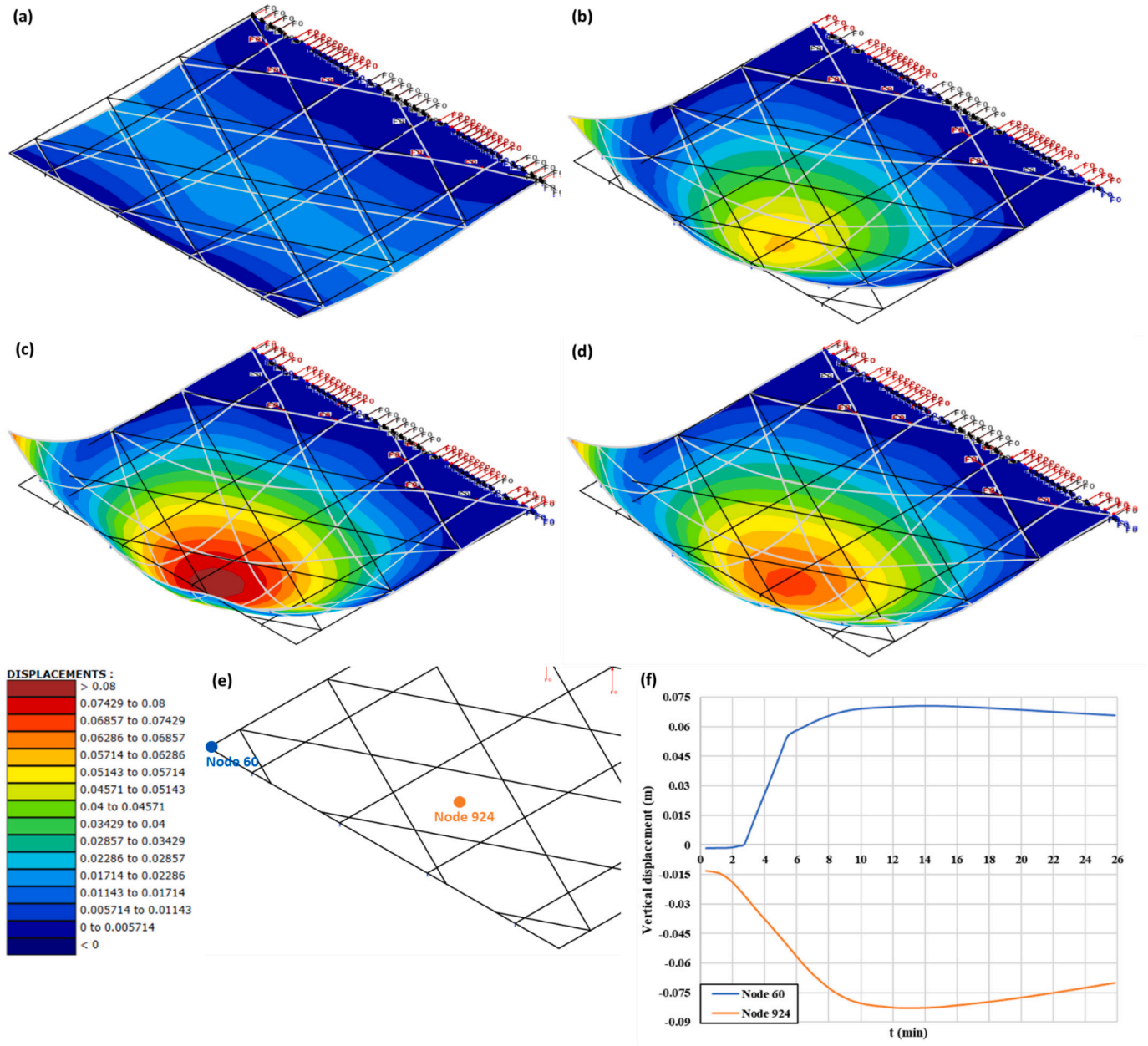

Fig. 18. Vertical displacement results during the fire. Values range from 0 m (dark blue) to 0.08 m (dark red) represented in figures (a)-(d). (a) Vertical displacements after 2 min. (b) Vertical displacements after 6 min. (c) Vertical displacements after 12 min. (d) Vertical displacements after 27 min. (e) Location of Nodes 60 and 924 for reference. (f) Numerical results of vertical displacements for nodes 60 (blue) and 924 (red). (For interpretation of the references to colour in this figure legend, the reader is referred to the web version of this article.)

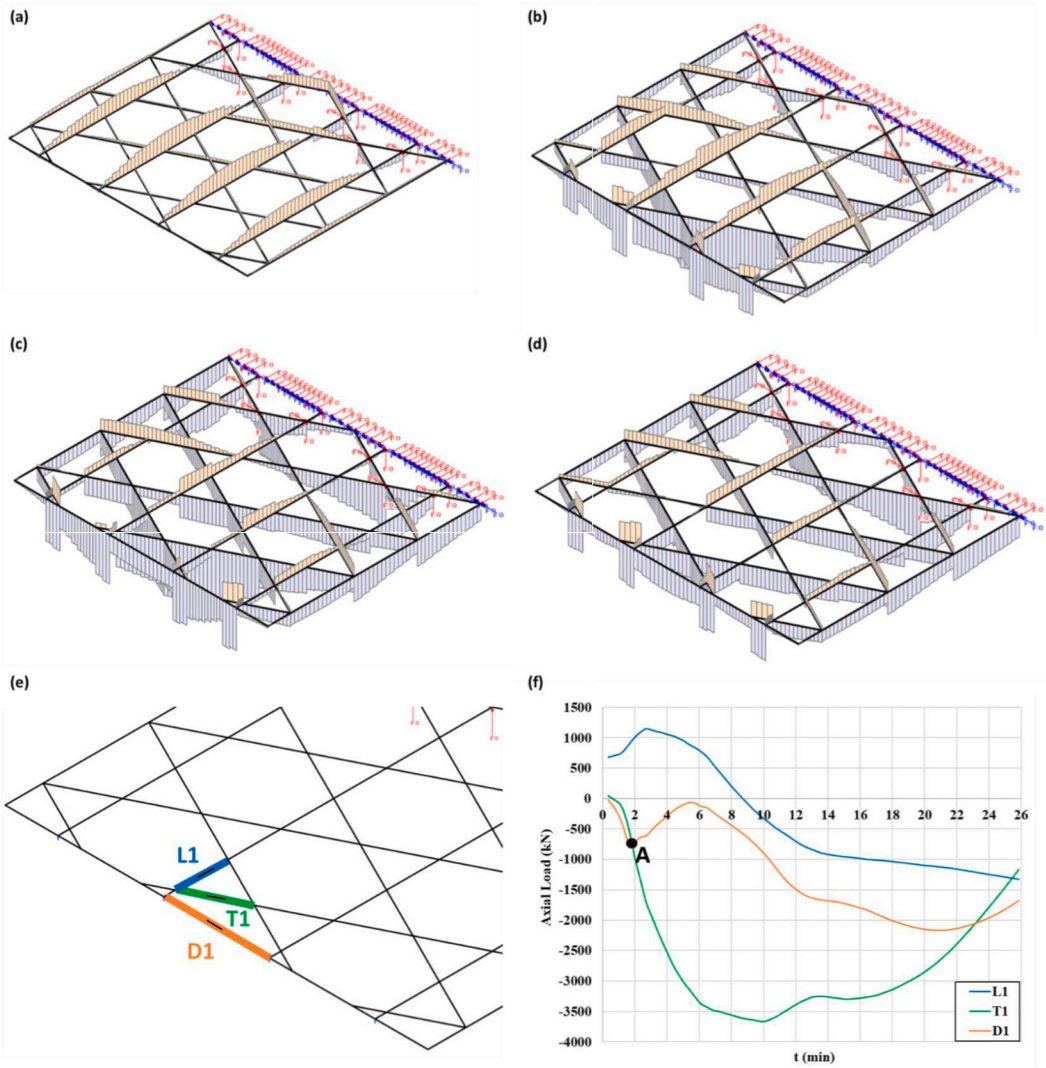

Fig. 19. Axial loads during the fire. Compression and tension are represented by blue and orange colour bars respectively in figures (a)-(d). (a) Axial loads at ambient temperature. (b) Axial loads after 6 min. (c) Axial loads after 12 min. (d) Axial loads after 25 min. (e) Location of most affected beam elements. (f) Numerical results of axial loads for most affected beam elements. Negative values indicate compression forces and positive values indicate tension forces. (For interpretation of the references to colour in this figure legend, the reader is referred to the web version of this article.)

min from the beginning of the fire and starts decaying after this point. As the section of diaphragm girder located above the fire and adjacent sections tend to expand due to the increasing temperatures, extreme nodes of this beam (e.g. node 60 in Fig. 18e and f) tend to expand laterally. However, longitudinal and transversal girders connected to the extreme sections of the diaphragm girder are not significantly heated and restrain this lateral displacement, forcing these extreme nodes to uplift to account for this expansion.

- In relation to the axial load, the following conclusions can be extracted from results:
  - o At ambient temperature, sections identified in Fig. 19e closest to the fire location were either in tension (elements T1 and L1) or under minimal compression (element D1). However, the fire and subsequent girders heating, provoked significant compression forces in them.
  - o It should be noted that transversal girders above the fire source (e.g. element T1) are heated at a similar rate than the central segment of Diaphragm Girder 1 and therefore they restrict its expansion to a much lesser extent than the longitudinal girders.
  - o Fig. 19 visually depicts the dynamic transformation of the central segment of the Diaphragm Girder 1 (represented by element D1). This segment, subjected to elevated temperatures, undergoes a swift shift from nearly zero axial load to a substantial compression. This transformation arises from the constraints imposed by the structural elements less affected by the fire at the outset, such as the Longitudinal Girder 1. In fact, Fig. 19 shows how the tension in these elements (see e.g. element L1) increases as the compression in element D1 rises until reaching a maximum around 2.5 min (point A in Fig. 19f). From that moment on, those girders opposing the free expansion of the central segment of Diaphragm Girder 1 start heating up and expand, relaxing the imposed restraint. This leads to a decrease in tension and subsequently initiates compression in Longitudinal Girder 1 (represented by its element L1). Over a 4-min period, there is a reduction of compression in the Diaphragm Girder 1. Once the fire fully develops (approximately after 6 min), the diaphragm girder heats up again more rapidly than the adjacent girders, and therefore, it has a greater tendency to expand, which introduces additional compressive forces in the Diaphragm Girder 1 (represented by element D1), in the Longitudinal Girder 1 (represented by element L1), and in the Transversal Girder 1 (represented by element T1).

- o Overall, there is a significant increase of compression along the steel girders located in the vicinity of the fire load (i.e. girders corresponding to elements D1, T1, L1 in Fig. 19e and their symmetric ones). These high compression forces together with the proportional limit reduction and the reduced stiffness due to the Young modulus reduction explain the local buckling observed on site along the web and bottom flange for the box-girder beams and bottom flange of the diaphragm girder.

4. Repair works

The repair works encompassed the following main tasks defined and supervised on-site by the construction management team (see Fig. 20):

- Restoring fire-affected concrete paraments and repairing all cracked welding.
- Replacing the fire-damaged section of the diaphragm girder.
- Replacing the pot bearings, which required temporarily raising the deck using hydraulic jacks and welding additional stiffeners to the diaphragm girder at the hydraulic jack locations.
- Levelling the bridge deck asphalt surface to match the pre-fire asphalt profile.
- Replacing the expansion joint.
- Conducting a load test after the completion of repair works to verify the bridge appropriate behaviour.

Both, the deck raising, and the load test were closely monitored using strain fiber optic sensors, LVDTs and conventional surveying techniques.

Numerical models played a crucial role in significantly reducing both the cost and time of repair works, a necessity given the pivotal role of the bridge in the city of Valencia. Specifically, numerical models confirmed the need to replace the pot bearings, confirmed the overall good condition of the steel material and shear connection after the fire, and highlighted the superficial nature of the concrete damage. However, due to the inherent complexity of the event and the limitations of the numerical models, their findings were complemented with a load test. This additional assessment validated the overall good condition of the bridge after the completion of repairs.

5. Lessons learnt

The following lessons have been learnt from the post-fire assessment of the bridge:

- It is imperative to emphasize the preservation of the fire event evidences because they are critical for an accurate estimation of the fire load, fire size, type of combustion, burning materials and boundary/ambient conditions which are key inputs of the fire model. This model is an essential part of the analysis and plays an important role in the reliability of results as it is the variable subjected to the highest level of uncertainty.
- Advanced numerical models, when complemented with experimental investigations like material tests and load tests, provide valuable insights for informed decisions regarding post-fire structural integrity. They can also contribute to substantial cost savings in repair efforts. However, it is essential to strike a balance between the time required for analysis and the costs associated with keeping a bridge closed, especially given the urgency to return bridges to service promptly.
- An interesting aspect deserving attention is the comparative performance of box-girders versus I-beams in fire scenarios. Box-girders tend to outperform I-beams due to their design and geometry. The enclosed shape of a box-girder acts as a thermal shield, protecting its internal components from extreme heat, resulting in slower temperature increases compared to I-beams directly exposed to fire. Additionally, the open shape of I-beams exposes more surface area to the fire, causing them to heat up and potentially weaken faster. Box-girders also typically have more mass than similarly sized I-beams, which serves as a heat sink, efficiently absorbing and dissipating heat, further delaying temperature rises within the box-girder. Furthermore, the geometry of box-girders, featuring two webs and two top flanges, enables the development of multiple load paths and provides increased redundancy compared to I-girders. As a result, even if a portion of the box-girder weakens due to heat, other parts can assume the structural load, making the box-girder more resistant to deformation and collapse. Finally, in the particular case studied in this paper, resilience was enhanced thanks to two decisions taken by the bridge designers: 1) steel members were designed to remain within the elastic range, meaning they were designed to function without undergoing yielding, for ultimate limit state load combinations, and 2) the complex geometry of the bridge, defined by longitudinal and transversal girders intersecting diagonally in plan, provides multiple load paths to transfer loads to the bridge supports. Consequently, it is conceivable that had the bridge employed I-beams, they might have required replacement.

6. Conclusions

Bridges are vital for transportation but susceptible to fire hazards. Despite this vulnerability, there is a lack of both experimental research and design guidelines for ensuring fire safety in bridges. This underscores the importance of studying actual bridge fire incidents.

This article presents a comprehensive overview of the numerical and experimental works carried out to evaluate the condition of a composite box-girder bridge located in the city of Valencia, Spain, following a fire incident. It also outlines the repair works undertaken to restore the bridge to full service. The following conclusions can be drawn from these studies:

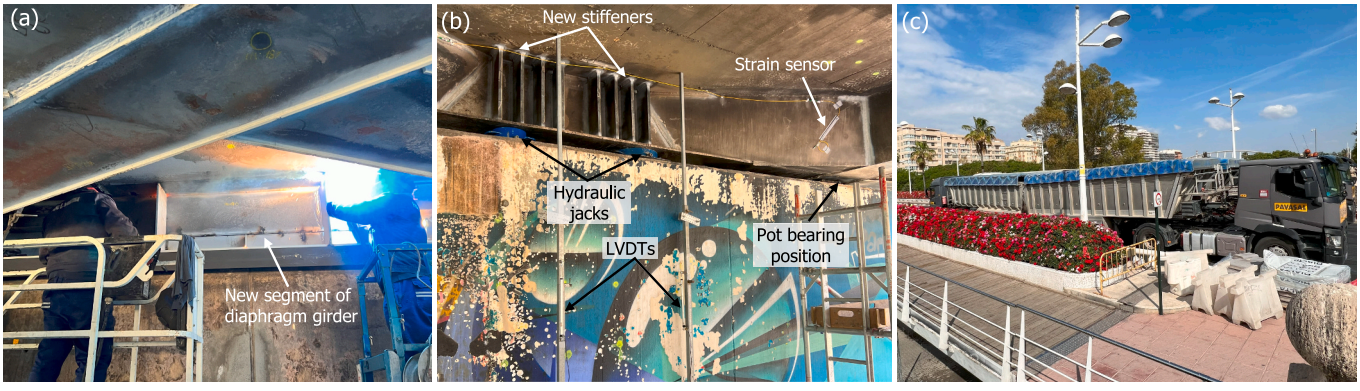

Fig. 20. Repair works: (a) Replacement of damaged section of the diaphragm girder. (b) Raise of the deck to enable pot bearings replacement. (c) Load test.

- Detailed assessments of the post-fire condition of the bridge, including concrete core testing, steel tensile tests, and 3D scanning, provided valuable guidance for repair and reinforcement efforts. While some areas of the bridge exhibited resilience, others faced structural challenges, emphasizing the importance of such assessments.
- The proposed multi-step approach (from natural fire model to non-linear 3D FE structural analysis) offered crucial insights at each step, strengthening the on-site hypotheses, and aiding on the repairing strategy. On this context, the study validated the fire model by comparing flame and smoke spread predictions with on-site observations. The model's ability to capture flame spread and smoke propagation was evident, aligning with site photos. The analysis also addressed concrete spalling, highlighting potential areas of concern.
- The heat transfer analysis provided a detailed understanding of temperature distributions within structural members. While some areas experienced significant temperature increases, the majority of elements maintained their structural integrity, with steel reinforcement remaining robust. However, local buckling was observed in steel girders subjected to higher temperatures.
- Furthermore, the mechanical response analysis shed light on the behaviour of the bridge during the fire. The bridge exhibited stability during the entire fire scenario, and the analysis revealed insights into vertical deflections and axial load changes, contributing to the understanding of its structural performance under fire conditions.
- The lessons learnt emphasize critical aspects of fire safety for bridges. Preserving fire event data is paramount for accurate fire modelling, reducing uncertainty in structural assessments. The combination of advanced numerical models and experimental investigations offers cost-effective ways to evaluate post-fire structural integrity. Additionally, the comparative performance analysis of box-girders versus I-beams underscores the advantages of box-girders in fire scenarios.

This study has shed light on critical aspects of bridge safety under fire conditions, and its findings are very valuable for all the stakeholders involved in the improvement of bridge resilience. Future research efforts should prioritize the following:

- Comparing the accuracy of the structural fire engineering results when adopting more complex approaches. This could involve using beam models incorporating the effects of instabilities with a modified effective stress in compression for steel girders (see e.g. [47]), using models with only shell or solid elements, or exploring new design methodologies as those proposed by [48,49].
- Conducting a comparative analysis of the fire response between I-girders and box-girders with equivalent mechanical capacity to quantify their different fire response as suggested by lessons learnt from the case study.

CRediT authorship contribution statement

Juan José Pagán-Martínez: Conceptualization, Data curation, Formal analysis, Investigation, Methodology, Software, Visualization, Writing – original draft. **Ignacio Paya-Zaforteza:** Conceptualization, Data curation, Formal analysis, Funding acquisition, Investigation, Methodology, Project administration, Writing – review & editing. **Antonio Hospitaler-Pérez:** Conceptualization, Formal analysis, Investigation, Methodology, Writing – review & editing.

Declaration of Competing Interest

The authors declare the following financial interests/personal relationships which may be considered as potential competing interests:

Ignacio Paya-Zaforteza reports financial support was provided by Pavasal Empresa Constructora S.A. If there are other authors, they declare that they have no known competing financial interests or personal relationships that could have appeared to influence the work reported in this paper.

Data availability

The authors do not have permission to share data.

Acknowledgements

This work has been made possible through the support of the “Service of Works Management and Infrastructure Maintenance of Valencia City Council” and the companies “Pavasal Empresa Constructora S.A.” and “ICEV Ingeniería de Estructuras”.

References

[1] G.M. Calvi, M. Moratti, G.J. O'Reilly, N. Scattarreggia, R. Monteiro, D. Malomo, et al., Once upon a time in Italy: the tale of the Morandi bridge, Struct. Eng. Int. 29 (2019) 198–217, https://doi.org/10.1080/10168664.2018.1558033.
[2] The I-35W Bridge Collapse, What Happened, What's Changed - CBS Minnesota. https://www.cbsnews.com/minnesota/news/bridge-collapse-whats-changed/, 2017.
[3] M. Garlock, I. Paya-Zaforteza, V. Kodur, L. Gu, Fire hazard in bridges: review, assessment and repair strategies, Eng. Struct. 35 (2012) 89–98, https://doi.org/10.1016/j.engstruct.2011.11.002.
[4] Z. Liu, G.-Q. Li, I. Paya-Zaforteza, C.S. Cai, Q. Huang, Fire hazards in bridges: state of the art, recent Progress, and current research gaps, J. Bridg. Eng. 28 (2023) 03123003, https://doi.org/10.1061/JBENF2.BEENG-5790.
[5] Z. Zhu, S.E. Quiel, N.E. Khorasani, Bivariate structural-fire fragility curves for simple-span overpass bridges with composite steel plate girders, Struct. Saf. 100 (2023) 102294, https://doi.org/10.1016/j.strusafe.2022.102294.
[6] C.S. Bajwa, E.P. Easton, H. Adkins, J. Cuta, N. Klymyshyn, S. Suffield, The MacArthur Maze Fire and Roadway Collapse: A “Worst Case Scenario” for Spent Nuclear Fuel Transportation? Volume 7: Operations, Applications and Components, American Society of Mechanical Engineers, Toronto, Ontario, Canada, 2012, pp. 261–269, https://doi.org/10.1115/PVP2012-78637.
[7] M. Yang, N. Badshah, T. Ambrose, M. Bryant, A. Fulton, Three Killed as Huge Explosion Causes Key Crimea-Russia Road Bridge to Collapse – As it Happened, The Guardian, 2022.
[8] E. Rivault, Crimea Bridge: How Russia is Rebuilding its Vital Link, BBC News, 2022.
[9] M. Catalini, M. Levy, In Rubble Beneath I-95 Collapse in Philadelphia, Investigators Looking for Truck Fire's Cause, Nationalpost, 2023. https://nationalpost.com/news/world/long-commutes-start-after-part-of-i-95-collapses-in-philadelphia-following-tanker-truck-fire (accessed June 22, 2023).
[10] H. Ingason, Y.Z. Li, A. Lönnermark, Tunnel Fire Dynamics, New York, NY, Springer New York, 2015, https://doi.org/10.1007/978-1-4939-2199-7.
[11] K. LaMalva, D. Hopkin (Eds.), International Handbook of Structural Fire Engineering, Springer International Publishing, Cham, 2021, https://doi.org/10.1007/978-3-030-77123-2.
[12] P. Rinaudo, I. Paya-Zaforteza, P.A. Calderón, Improving tunnel resilience against fires: a new methodology based on temperature monitoring, Tunn. Undergr. Space Technol. 52 (2016) 71–84, https://doi.org/10.1016/j.tust.2015.11.021.
[13] Y. Cao, J. Jiang, Y. Lu, W. Chen, J. Ye, Progressive collapse of steel structures exposed to fire: a critical review, J. Constr. Steel Res. 207 (2023) 107985, https://doi.org/10.1016/j.jcsr.2023.107985.
[14] M.M. Drury, S.E. Quiel, Standard versus natural fire resistance for partially restrained composite floor beams: 1-testing, J. Constr. Steel Res. 202 (2023) 107768, https://doi.org/10.1016/j.jcsr.2022.107768.
[15] W. Yang, Y. Yang, F. Liu, Y.F. Chen, Fire research of joint between special-shaped CFST column and U-shaped composite beam, J. Constr. Steel Res. 213 (2024) 108349, https://doi.org/10.1016/j.jcsr.2023.108349.
[16] J. Alos-Moya, I. Paya-Zaforteza, A. Hospitaler, P. Rinaudo, Valencia bridge fire tests: experimental study of a composite bridge under fire, J. Constr. Steel Res. 138 (2017) 538–554, https://doi.org/10.1016/j.jcsr.2017.08.008.
[17] J. Hu, R. Carvel, A. Usmani, Bridge fires in the 21st century: a literature review, Fire Saf. J. 126 (2021) 103487, https://doi.org/10.1016/j.firesaf.2021.103487.
[18] B. Nicoletta, P. Kotsovinos, J. Gales, Review of the fire risk, hazard, and thermomechanical response of bridges in fire, Can. J. Civ. Eng. 47 (2020) 363–381, https://doi.org/10.1139/cjce-2018-0767.
[19] N. Hua, A. Tessari, Khorasani N. Elhami, Characterizing damage to a concrete liner during a tunnel fire, Tunn. Undergr. Space Technol. 109 (2021) 103761, https://doi.org/10.1016/j.tust.2020.103761.
[20] Ministerio de Fomento, Recomendaciones para el proyecto de puentes mixtos para carreteras RPX-95, 1996.
[21] J. Alos-Moya, I. Paya-Zaforteza, A. Hospitaler, E. Loma-Ossorio, Valencia bridge fire tests: validation of simplified and advanced numerical approaches to model bridge fire scenarios, Adv. Eng. Softw. 128 (2019) 55–68, https://doi.org/10.1016/j.advengsoft.2018.11.003.
[22] J. Alos-Moya, I. Paya-Zaforteza, M.E.M. Garlock, E. Loma-Ossorio, D. Schiffner, A. Hospitaler, Analysis of a bridge failure due to fire using computational fluid

dynamics and finite element models, Eng. Struct. 68 (2014) 96–110, https://doi.org/10.1016/j.engstruct.2014.02.022.
[23] K. McGrattan, Verification and Validation of Selected Fire Models for Nuclear Power Plant Applications Vol. 7, Fire Dynamics Simulator, 2007.
[24] K. McGrattan, Heat Release Rates of Multiple Transient Combustibles, National Institute of Standards and Technology, Gaithersburg, MD, 2020, https://doi.org/10.6028/NIST.TN.2102.
[25] M.J. Hurley (Ed.), SFPE Handbook of Fire Protection Engineering, Fifth edition, Springer, New York, 2016.
[26] CEN, Eurocode 2: Design of Concrete Structures - Part 1–2: General Rules - Structural Fire Design, 2005.
[27] CEN, Eurocode 3: Design of Steel Structures - Part 1–2: General Rules - Structural Fire Design, 2005.
[28] G. Peris-Sayol, I. Paya-Zaforteza, J. Alos-Moya, A. Hospitaler, Analysis of the influence of geometric, modeling and environmental parameters on the fire response of steel bridges subjected to realistic fire scenarios, Comput. Struct. 158 (2015) 333–345, https://doi.org/10.1016/j.compstruc.2015.06.003.
[29] Observación meteorológica en VALENCIA VIVEROS el domingo 4 de diciembre de 2022. https://x-y.es/aemet/est-8416Y-valencia-viveros?fecha=2022-12-04, 2023 (accessed December 3, 2023).
[30] The Beaufort Wind Scale, RMetS. https://www.rmets.org/metmatters/beaufort-wind-scale, 2023 (accessed December 3, 2023).
[31] U. Wickström, D. Duthinh, K.B. McGrattan, Adiabatic Surface Temperature for Calculating Heat Transfer to Fire Exposed Structures, NIST, 2007.
[32] J.-M. Franssen, T. Gernay, Modeling structures in fire with SAFIR: theoretical background and capabilities, JSFE 8 (2017) 300–323, https://doi.org/10.1108/JSFE-07-2016-0010.
[33] CEN, Eurocode 1: Actions on Structures - Part 1–2: Actions on Structures Exposed to Fire, 2002.
[34] D. Talamona, A quadrangular Shell finite element for concrete and steel structures subjected to fire, J. Fire. Prot. Eng. 15 (2005) 237–264, https://doi.org/10.1177/1042391505052769.
[35] W. Wang, G. Li, S. Chen, Experimental study on fire resistance of steel bar truss slab and steel composite beams, China Civ. Eng. J. 48 (2015) 67–75.
[36] S. Pfenning, J. Tresch, L. Pennisi, S. Brunkhorst, M. Mensinger, Influence of the degree of shear connection on the load carrying capacity of a composite beam in fire, Ce Papers 1 (2017) 477–486, https://doi.org/10.1002/cepa.547.
[37] O. Vassart, B. Zhao, Fire Resistance Assessment of Partially Protected Composite Floors, FRACOF. Design Guide, 2011.
[38] O. Vassart, M. Hawes, W.I. Simms, B. Zhao, J.-M. Franssen, A. Nadjai, Fire Resistance of Long Span Cellular Beam Made of Rolled Profiles, FICEB. Final Report, 2010.
[39] O. Vassart, B. Zhao, Membrane Action of Composite Structures in Case of Fire. MACS+. Design Guide, 2012.
[40] M. Drury, Numerical Investigation of Composite Floor Beam Resilience to Realistic Fire Scenarios, Lehigh University, 2019.
[41] CEN, Eurocode 4. Design of Composite Steel and Concrete Structures. Part 1–2: General Rules - Structural Fire Design, 2008.
[42] O. Mirza, B. Uy, S. Krezo, Experimental studies on the behaviour of headed stud shear connectors for composite steel concrete beams under elevated temperatures, Steel Aluminium Struct. Res. Publish. Serv. (2011) 467–473, https://doi.org/10.3850/978-981-08-9247-0_rp066-icsas11.
[43] T. Gernay, A. Millard, J.-M. Franssen, A multiaxial constitutive model for concrete in the fire situation: theoretical formulation, Int. J. Solids Struct. 50 (2013) 3659–3673, https://doi.org/10.1016/j.ijsolstr.2013.07.013.
[44] SOFiSTiK FEM, BIM and CAD Software for Structural Engineers. https://www.sofistik.com/, 2023 (accessed September 21, 2023).
[45] Company I, Puente de las Flores (Valencia). IN-06. Prueba de Carga Vano 8, 2023.
[46] CEN, Eurocode 4. Design of Composite Steel and Concrete Structures. Part 1–1: General Rules and Rules for Buildings, 2004.
[47] J. Franssen, B. Cowez, T. Gernay, Effective stress method to be used in beam finite elements to take local instabilities into account, Fire Saf. Sci. 11 (2014) 544–557, https://doi.org/10.3801/IAFSS.FSS.11-544.
[48] M.R. Pallares-Muñoz, I. Paya-Zaforteza, A. Hospitaler, A new methodology using beam elements for the analysis of steel frames subjected to non-uniform temperatures due to fires, Structures 31 (2021) 462–483, https://doi.org/10.1016/j.istruc.2021.02.008.
[49] M.R. Pallares-Muñoz, I. Payá-Zaforteza, A. Hospitaler-Pérez, New modeling strategies for analyzing lateral-torsional buckling in class-4 steel structural members at elevated temperatures using beam-type elements, Structures 34 (2021) 3508–3532, https://doi.org/10.1016/j.istruc.2021.09.087.